Recent progress on optomagnetic coupling and optical manipulation based on cavity-optomagnonics

Kai Wang[1], Yong-Pan Gao[2], Rongzhen Jiao[1], Chuan Wang[3,†]

1   School of Science and the State Key Laboratory of Information Photonics and Optical Communications,
    Beijing University of Posts and Telecommunications, Beijing 100876, China
2   School of Electronic Engineering and the State Key Laboratory of Information Photonics and Optical Communications,
    Beijing University of Posts and Telecommunications, Beijing 100876, China
3   School of Artificial Intelligence, Beijing Normal University, Beijing 100875, China
    Corresponding author. E-mail: †wangchuan@bnu.edu.cn
    Received November 23, 2021; accepted March 30, 2022

ABSTRACT

Recently, the photon–magnon coherent interaction based on the collective spins excitation in ferromagnetic materials has been achieved experimentally. Under the prospect, the magnons are proposed to store and process quantum information. Meanwhile, cavity-optomagnonics which describes the interaction between photons and magnons has been developing rapidly as an interesting topic of the cavity quantum electrodynamics. Here in this short review, we mainly introduce the recent theoretical and experimental progress in the field of optomagnetic coupling and optical manipulation based on cavity-optomagnonics. According to the frequency range of the electromagnetic field, cavity optomagnonics can be divided into microwave cavity optomagnonics and optical cavity optomagnonics, due to the different dynamics of the photon–magnon interaction. As the interaction between the electromagnetic field and the magnetic materials is enhanced in the cavity-optomagnonic system, it provides great significance to explore the nonlinear characteristics and quantum properties for different magnetic systems. More importantly, the electromagnetic response of optomagnonics covers the frequency range from gigahertz to terahertz which provides a broad frequency platform for the multi-mode controlling in quantum systems.

Keywords optomagnetic coupling, manipulation, cavity-optomagnonics, photon–magnon interaction

Contents

1   Introduction

The magnetic field is expressed by vector field that describes the magnetic influence on moving electric charges and magnetic materials in electromagnetics. It is used

throughout modern science and technology, particularly in electrical engineering and electromechanics. During the past years, magnetism is widely studied from compass, hard disc drives, to nuclear magnetic resonance(NMR) and magnetic resonance imaging [1], which shows broad applications in information science and medical science. However, as a key element of the electromagnetic field, the magnetic dipole moment in the medium is usually two orders of magnitude weaker than the electric dipole moment. Therefore, the electromagnetic–magnetic interaction is often ignored when going through the electromagnetic-matter interaction process. Due to the rapid development of the nano-technology, recent works show the performance of strong magnetic dipole interaction existed in the microwave cavity and ferromagnetic materials hybrid systems [2–6]. In these related systems, the collective excitation of spins in the ferromagnetic materials could construct the spin wave, and the quantized spin wave could be considered as the quasi-particle magnons. And the magnons, microwave photons can be strongly coupled through magnetic dipole interaction [2–11]. Meanwhile, the photon–magnon interaction could promote the conversion between microwaves and optical waves [12–14].

The related research has recently formed a new research field called cavity optomagnonics. According to the frequency range, cavity optomagnonics can be divided into the microwave cavity optomagnonics and the optical cavity optomagnonics. In 2010, Soykal and Flatté theoretically predicted several THz coupling terms in a ferromagnetic optomagnonical system [2, 3]. Subsequently, the experimental realization of strong optomagnonical coupling has become an interesting topic. In 2013, Huebl *et al.* constructed a hybrid quantum system using a sample of yttrium iron garnet (YIG) and a superconducting cavity [4]. They measured the transmission of the microwave signals, and found the modes anti-crossing effect, for which they assert the strong coupling of microwave photons and magnons. With the development of the optomagnonical systems on the microwave frequency range, several interesting phenomena have been observed, such as the magnons Kerr effect [15–18], non-Hermitian physics [19–26], optical chaos [27, 28], and dissipative coupling [29–39].

Specifically, the absorption spectrum of the YIG material is consistent with the commonly used optical communication wavelength, the optical whispering gallery mode of YIG sphere can also be excited in the hybrid system. In the YIG microsphere, the optical photons can be coupled with the magnons through Faraday effect, and the photon–magnon interaction can be detected by the optical transmission spectrum. When the triple resonance condition is fulfilled, the Brillouin scattering effect can be observed [7, 9, 10]. However, the photon–magnon coupling strength is only several Hertz for the small modes overlap. To further enhance the coupling strength, it is necessary to increase the mode overlap between the optical-photons and the magnons, such as the coupling of high-order magnon modes [40–43], designing the novel nanos-

Table 1 Some symbols used in this review.

Symbol	Meaning
$\boldsymbol{M}$	Magnetization
$\boldsymbol{\hat{S}}$	Macrospin $\boldsymbol{\hat{S}} = \boldsymbol{M}V_m/\gamma$
M_s	Saturation magnetization
γ	Gyromagnetic ratio
α	Gilbert damping constant
B_0	External bias magnetic field
$\hat{m}$ ($\hat{m}^\dagger$)	Magnon annihilation (creation) operator
$\hat{a}$ ($\hat{a}^\dagger$)	Photon annihilation (creation) operator
$\hat{a}_{\text{TE}}$ ($\hat{a}_{\text{TE}}^\dagger$)	TE photon mode annihilation (creation) operator
$\hat{a}_{\text{TM}}$ ($\hat{a}_{\text{TM}}^\dagger$)	TM photon mode annihilation (creation) operator
ω_m	Magnon resonant frequency $\omega_m = \gamma B_0$
ω_c	Cavity resonant frequency
g	Photon–magnon coupling strength
G	Microscopic magneto–optical coupling strength
V_m	Volume of the YIG sphere

tructures [13, 44–49]. Based on the efficient coupling between photons and magnons, more interesting phenomena could be realized, such as the tuning of magnons using optical field, and the nonlinear effects could be induced [50–55], which also provides novel methods for constructing tunable hybrid quantum systems.

Recently, the developments of quantum computers and quantum information processing focus on the large scale integration of qubits and manipulation with high fidelity. On the other hand, the hybrid quantum system may combine advantages in different systems which brings an effective way to break through the bottleneck of qubits manipulation, such as the emergence of cavity optomagnonics that build a platform to bridge the optical field with the magnetic systems. Here in this short review, we mainly introduce some recent research progress of optomagnetic coupling and optical manipulation based on cavity-optomagnonics. And a list of symbols in this review is given in Table 1. We believe that this review can provide a reference for the development of quantum computing based on composite systems in the future.

2 Spin wave and photon–magnon interaction

The spin wave is defined as a collective excitation of spins under ordered magnetic moment, and the quantized spin wave could be represented by the magnons. To further study the features of the spin waves, we present the Landau–Lifshitz–Gilbert (LLG) equations on the model of a yttrium iron garnet (YIG) sphere in this section.

The magnetism is contributed by the net magnetic dipole moment $\boldsymbol{\mu}$ of the atoms, so the magnetic dipole moment per volume could be described by the magnetiza-

tion M with the expression as [56]

$$M = \frac{\sum_i \boldsymbol{\mu}_i}{\delta V}. \tag{1}$$

The magnetization process of the material will induce the Zeeman interaction, demagnetizing field, magnetocrystalline anisotropy and exchange interaction [56]. The Zeeman interaction energy depends on the external static magnetic field $\boldsymbol{H}_{ext}$, and the energy density could be described as

$$E_z = -\mu_0 \boldsymbol{M} \cdot \boldsymbol{H}_{ext}, \tag{2}$$

where μ_0 denotes the vacuum permeability.

The magnetization process is usually accompanied by the generation of a demagnetizing field. And the demagnetizing field depends on the geometry of the material. For a highly symmetrical sphere, the demagnetizing field is $H_d = M_s/3$.

The magnetocrystalline anisotropy originates from the spin–orbit interaction. For uniaxial crystals, the effective magnetocrystalline anisotropy magnetic field $\boldsymbol{H}_{ani}$ could be described as

$$\boldsymbol{H}_{ani} = \frac{2K_1}{\mu_0 M_s}\left(\boldsymbol{u} \cdot \frac{\boldsymbol{M}}{M_s}\right)\boldsymbol{u} + \frac{4K_2}{\mu_0 M_s}\left(\boldsymbol{u} \cdot \frac{\boldsymbol{M}}{M_s}\right)^3 \boldsymbol{u}, \tag{3}$$

where K_1 and K_2 are the first-order and second-order anisotropy constants, respectively. $\boldsymbol{u}$ is the easy axis, which refers to the magnetization direction of the lowest energy. When only the linear region is taken into consideration, the anisotropic energy remanins constant. In the non-linear region, the anisotropic energy will induce the magnon Kerr effect [15]. The exchange interaction describes the interaction between the adjacent magnetic dipoles, and the effective exchange interaction field can be written as

$$\boldsymbol{H}_{ex} = l_{ex}^2 \Delta \boldsymbol{M}. \tag{4}$$

Here l_{ex} is the exchange length and Δ denotes the Laplace operator. For the long-wave spin waves, such as the Kittel mode, the exchange interaction energy keeps a constant.

Considering the interactions in magnetic material, the dynamic equations in magnetic media could be described by the LLG equation as [57, 58]

$$\frac{\mathrm{d}\boldsymbol{M}}{\mathrm{d}t} = -\gamma\mu_0(\boldsymbol{M} \times \boldsymbol{H}_{eff}) + \frac{\alpha}{M_s}\left(\boldsymbol{M} \times \frac{\mathrm{d}\boldsymbol{M}}{\mathrm{d}t}\right), \tag{5}$$

where $\boldsymbol{H}_{eff}$ denotes the effective magnetic field, which includs the external static magnetic field and the internal magnetic interaction field. The first term on the rhs of the Eq. (5) represents the precession of the magnetization around the effective magnetic field; the second term represents the attenuation of the precession. The LLG equation describes the spiral precession of the magnetization around the background magnetization as shown in Fig. 1(a). The precession of magnetization on different site influences each other and a spin wave could be formed which is shown in Fig. 1(b). Here we focus on the ferromagnetic resonance (FMR) mode, also known as the Kittel mode. The phases of all the spin precessions in this mode are the same, so it can be regarded as a spin wave with infinite wavelength, that is, the spin wave vector is zero. Then, the Hamiltonian $\hat{H}_{\mathrm{YIG}}$ of the Kittel mode in the YIG sphere can be written as

$$\hat{H}_{\mathrm{YIG}} = -\int_{V_m} \boldsymbol{M} \cdot \boldsymbol{B}_0 \mathrm{d}v, \tag{6}$$

where $\boldsymbol{B}_0 = B_0 \boldsymbol{e}_z$ is the external bias magnetic field applied along the z direction of the YIG sphere. By replacing the magnetization $\boldsymbol{M}$ with the macroscopic spin operator $\boldsymbol{S}$, Eq. (6) can be simplified to

$$\hat{H}_{\mathrm{YIG}} = -\gamma B_0 \hat{S}_z. \tag{7}$$

Considering the Holstein–Primakoff transformation [60], we have

$$\hat{S}_z = S - \hat{m}^\dagger \hat{m}, \tag{8}$$
$$\hat{S}^+ = \sqrt{2S - \hat{m}^\dagger \hat{m}}\,\hat{m},$$
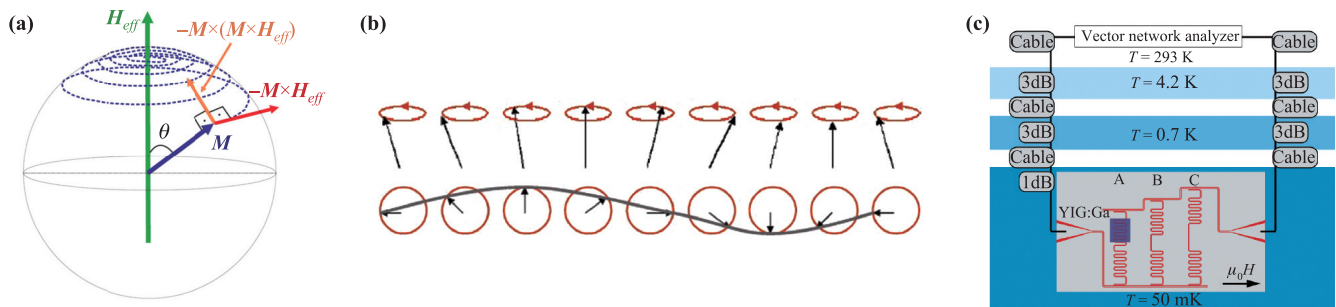$$\hat{S}^- = \hat{m}^\dagger \sqrt{2S - \hat{m}^\dagger \hat{m}}.$$

Fig. 1 Schematic diagram of magnetization dynamics, spin wave and microwave photon–magnon coupling system. **(a)** The magnetization precession process around the effective magnetic field [56]. Due to the damping term, the magnetization eventually tends to be equilibrium. The entire precession process corresponds to Eq. (5). **(b)** A spin wave excited on a one-dimensional spin chain when the magnetization is non-uniformly precessing [59]. **(c)** The first microwave cavity optomagnonical system. The gallium-doped YIG sample is coupled with the superconducting microwave cavity, and the whole experiment is carried out at cryogenic [4].

Kai Wang, et al., Front. Phys. 17(4), 42201 (2022)

42201-3

Here the macroscopic spin operator can be connected with the creation operator $\hat{m}^\dagger$ and annihilation operator $\hat{m}$ of the magnon, and Eq. (7) can be rewritten as

$$\hat{H}_{\text{YIG}} = \omega_m \hat{m}^\dagger \hat{m}, \tag{9}$$

where $\omega_m = \gamma B_0$ is the resonant frequency of the magnons.

Soykal and Flatté first theoretically discussed the possibility of realizing the strong interaction between magnons and microwave photons, and presented the full quantum Hamiltonian of the microwave cavity optomagnonical system [2, 3]. They also recommended the advantages of using YIG spheres for its large spin densities and low dissipation rate. Subsequently, Huebl et al. demonstrated the strong coupling between the magnons and the microwave photons for the first time [4]. The experiment was carried out with the YIG sample and a superconducting coplanar microwave resonator shown in Fig. 1(c) in the cryogenic environment. This experiment promoted the development of the microwave cavity optomagnonics and the optical cavity optomagnonics that appeared later. Specifically, the photon–magnon interaction in microwave cavity and optical cavity is essentially different. In the microwave cavity optomagnonic, there is a huge magnetic dipole interaction between the magnon and the microwave-photon. The interaction Hamiltonian can be described as ($\hbar = 1$)

$$\hat{H}_{int-m} = g(\hat{a}^\dagger \hat{m} + \hat{a}\hat{m}^\dagger), \tag{10}$$

which is similar to the beam–splitter interaction. However, in the optical cavity optomagnonics, photon–magnon coupling is the transition process between three energy levels. When the frequency difference between TE and TM photonic modes is exactly resonant with the magnon frequency, the interaction Hamiltonian can be written as ($\hbar = 1$)

$$\hat{H}_{int-o} = g(\hat{m}\hat{a}_{\text{TM}}\hat{a}_{\text{TE}}^\dagger + \hat{m}^\dagger \hat{a}_{\text{TM}}^\dagger \hat{a}_{\text{TE}}). \tag{11}$$

The photon–magnon coupling mechanism in optical cavity is the Faraday effect. However, when the spin cannot be replaced by a harmonic oscillator [50], the general interaction Hamiltonian can be expressed as (choosing $\hbar = 1$)

$$\hat{H}_{int} = G\hat{S}_x \hat{a}^\dagger \hat{a}. \tag{12}$$

Here $\boldsymbol{S} = (S_x, S_y, S_z)$ is the macrospin and G represents the microscopic magneto–optical coupling strength, which determined by the Faraday effect.

3 Microwave cavity-optomagnonics

In this section, we focus on the studies of the microwave cavity-optomagnonics. Due to the low and unstable quality factor of the superconducting microwave cavity in previous works, it limits the increasing of the coupling strength. Tabuchi and Zhang et al. used a three-dimensional copper cavity to achieve strong coupling between microwave photons and magnons at low temperature [5] and room temperature [6], respectively, to stabilize the quality factor of the microwave cavities. The mode distribution and frequency of the microwave cavity depend on the shape and size of the cavity. Goryachev et al. used a novel multiple-post reentrant cavity and achieved 2 GHz ultrastrong coupling [61]. Zhang et al. experimentally compared the different coherence characteristics of the device at cryogenic and room temperature [62]. Soon after, scientists began to study the nonlinear effects of the cavity optomagnonics. For example, by directly pumping the magnons, Wang et al. observed the magnonic Kerr nonlinear effect [15, 16].

3.1 Microwave photon–magnon strong coupling and ultrastrong coupling

Experimentally, the rectangular copper cavity is more stable than the superconducting cavity when coupled with the magnons. Two groups have achieved the strong coupling of the rectangular copper cavity and Kittel mode magnon at cryogenic [5] and room temperature [6], respectively. The experimental device and mode splitting spectrum are shown in Figs. 2(a), (b) and (d), (e). Cavity mode is weakly coupled with a small portion of the magnetostatic mode under the low temperature conditions [62]. By fitting the spectrum $S_{21}(\omega)$ or $S_{12}(\omega)$, the photon–magnon coupling strength, the linewidth of the cavity mode and the magnon mode can be obtained. Here the hybrid system can be described by the Hamiltonian ($\hbar = 1$) as

$$\hat{H} = \omega_c \hat{a}^\dagger \hat{a} + \omega_m \hat{m}^\dagger \hat{m} + g(\hat{a}^\dagger \hat{m} + \hat{a}\hat{m}^\dagger). \tag{13}$$

The photon–magnon coupling strength is related to the number of the net spins N. Assuming that all the net spins in the YIG sphere are precessed in phase, the photon–magnon coupling strength in Eq. (13) can be expressed as

$$g = g_0 \sqrt{N}, \tag{14}$$

where g_0 is the coupling strength of a single spin to the cavity, which is related to the mode volume of the microwave cavity and the gyromagnetic ratio. Tabuchi et al. used the YIG spheres with different diameters (that is, different spin numbers) to experimentally proved that the photon–magnon coupling strength is proportional to the square root of the number of spins [5], the result is shown in Fig. 2(c).

Since the strong coupling will induce the coherent dynamical conversion between photon and magnons and generate Rabi-like oscillation, by monitoring the time evolution of the cavity output field after a short pulse excitation, Zhang et al. experimentally obtained the time traces
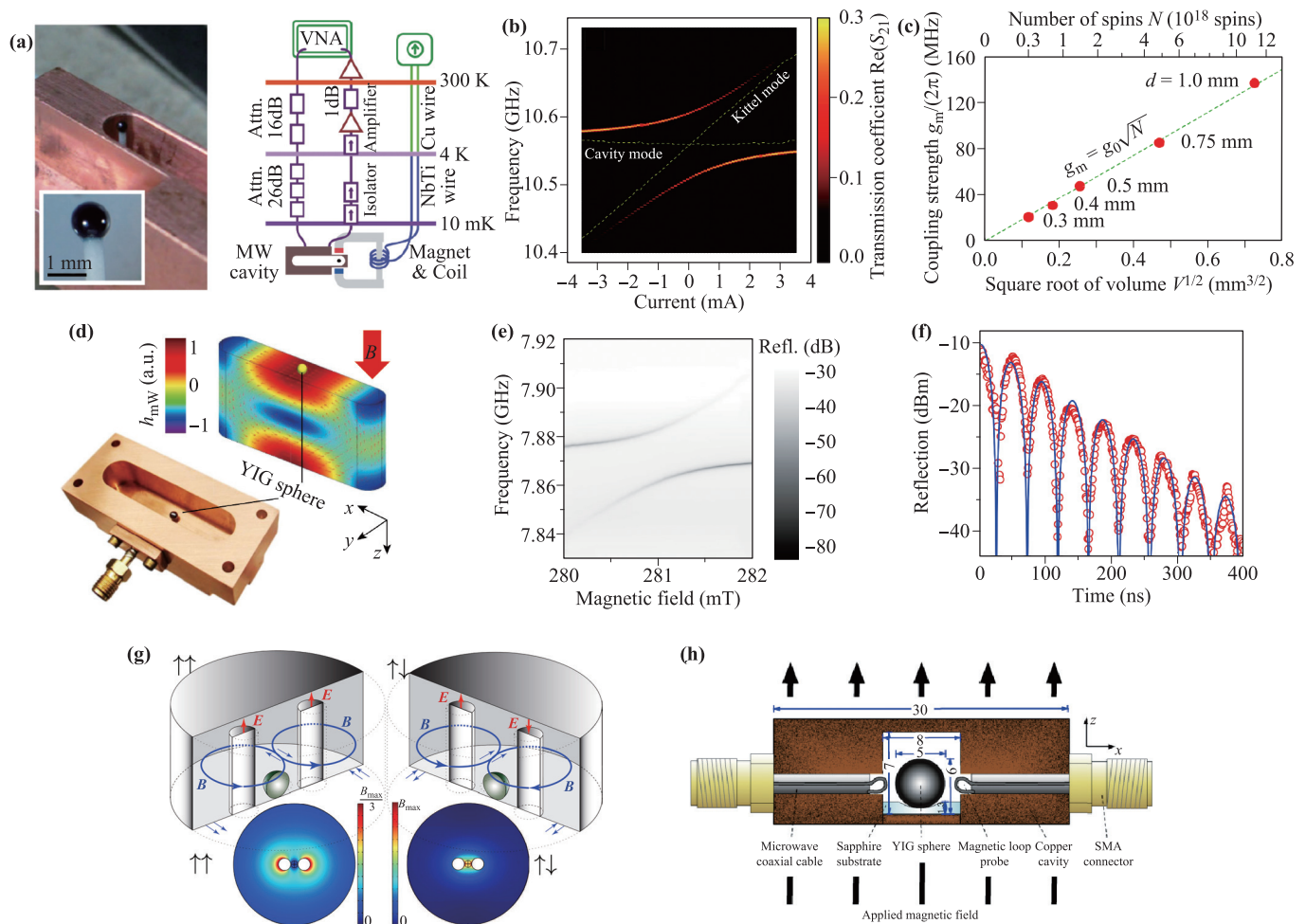
42201-4

Kai Wang, et al., Front. Phys. 17(4), 42201 (2022)

Fig. 2 Strong coupling and ultrastrong coupling system. **(a–c)** Microwave cavity optomagnonical system designed by Tabuchi *et al.* and some measurement results [5]. (a) Schematic diagram of rectangular microwave cavity and measurement proposal. The microwave cavity is made of oxygen free copper, and its fundamental mode TE_{101} resonant frequency is 10.565 GHz. The illustration is a YIG sphere with a diameter of 1 mm. (b) The measured normal mode splitting spectrum. Current I is used to tune the bias magnetic field of the YIG sphere. Reflects the change of the transmission spectrum S_{21} with the magnetic field. The anti-crossing feature represents the strong coupling between microwave photon and magnon. (c) The relationship between coupling strength and spin number. YIG sphere of different diameters are used to represent different spin numbers. **(d–f)** Microwave cavity optomagnonical system designed by Zhang *et al.* and some measurement results [6]. (d) Schematic diagram of the rectangular microwave cavity and the distribution of the fundamental mode TE_{101}. (e) The variation trend of reflection spectrum S_{11} with bias magnetic field. (f) By monitoring the time evolution of the reflection spectrum amplitude after short pulse excitation, Rabi oscillations are observed. **(g, h)** Microwave cavity optomagnonical system designed to achieve ultra-strong coupling [61, 64].

consistent with the theoretical prediction of Rabi-like oscillations, see Fig. 2(f). In the later work, they observed the magnetically induced transpancy (MIT) and the Purcell effect, which further proved the coherent coupling of microwave photons and magnons [6].

By optimizing the cavity parameters and increasing the spin numbers, the performance of coupling strength can continue to be improved [61, 63, 64]. For example, by reducing the size of the microwave cavity and increasing the diameter of the YIG sphere, Zhang *et al.* achieved an ultrastrong coupling with $g/(2\pi) = 2.5$ GHz in a microwave cavity with resonance frequency of 37.5 GHz [6]. Goryachev *et al.* used a novel multiple-post reentrant cav-

ity to effectively focusing the resonant magnetic field into the YIG crystal, and achieved a very large filling factor at microwave frequencies [61] which also obtained 2 GHz coupling strength. By placing a 5 mm diameter YIG sphere in a cylindrical copper cavity [64], Bourhill *et al.* achieved 7.11 GHz optical–magnetic coupling intensity. The detailed experimental devices are shown in Figs. 2(g) and (h).

The above researches have initially demonstrated the superiority of the magnons. Magnon tuning is expected to bring the technological revolution and promote the development of basic physics. In next subsection, we will introduce some interesting phenomena based on the photon–

magnon interaction.

3.2 The cryogenic and room temperatures optomagnonics

The strong coupling between the microwave photons and the magnons has been observed at both cryogenic and room temperature conditions. An interesting question is often been asked: what does the temperature affect during the coupling process?

To response this issue, Zhang *et al.* measured the transmission spectrum of the same system at cryogenic and room temperature, respectively [62]. The current microwave cavity has two resonance modes, say the TE_{101} mode and the TE_{102} mode. The simulated magnetic field distribution in the microwave cavity is shown in Fig. 3(a). By coupling the YIG sphere to these two modes respectively, the measured transmission spectrum are shown in Figs. 3(b)–(e). Here Figs. 3(b) and (c) are transmission spectra measured at cryogenic, while Figs. 3(d) and (e) are the conditions at room temperatures. These results show that the temperature will not change the coupling

strength. However, it is different for the magnetostatic mode for which the strong coupling can be achieved at cryogenic while disappeared at room temperature. The transmission spectrum of the hybrid system can be written as

$$S_{21}(\omega) = \frac{2\sqrt{\kappa_i \kappa_o}}{\mathrm{i}(\omega - \omega_c) - \kappa_{tot} + \sum(\omega)}, \quad (15)$$

where $\kappa_i (\kappa_o)$ is the input (output) loss rate. $\kappa_{tot} = \kappa_i + \kappa_o + \kappa_{int}$ represents the total cavity decay rate, here κ_{int} is the intrinsic decay rate of the microwave cavity. $\sum(\omega) = \frac{\tilde{g}_{FMR}^2}{\mathrm{i}(\omega - \omega_{FMR}) - \gamma_{FMR}} + \frac{\tilde{g}_{MR}^2}{\mathrm{i}(\omega - \omega_{MR}) - \gamma_{MR}}$, where $\omega_{FMR} (\omega_{MR})$ is the resonance frequency of the FMR (MR) mode. And $\tilde{g}_{FMR}^2 (\tilde{g}_{MR}^2)$ is the magnon–photon coupling strength corresponding to the FMR (MR) mode. $\gamma_{FMR} (\gamma_{MR})$ denotes the decay rate of the FMR (MR) mode.

The MS mode has low dissipation rate at cryogenic, and the experimental results are fit well with the theoretical predictions. At room temperature, the magnetostatic mode is decoupled from the cavity when the dissipation of the MS mode is increased, the results can also fit well.
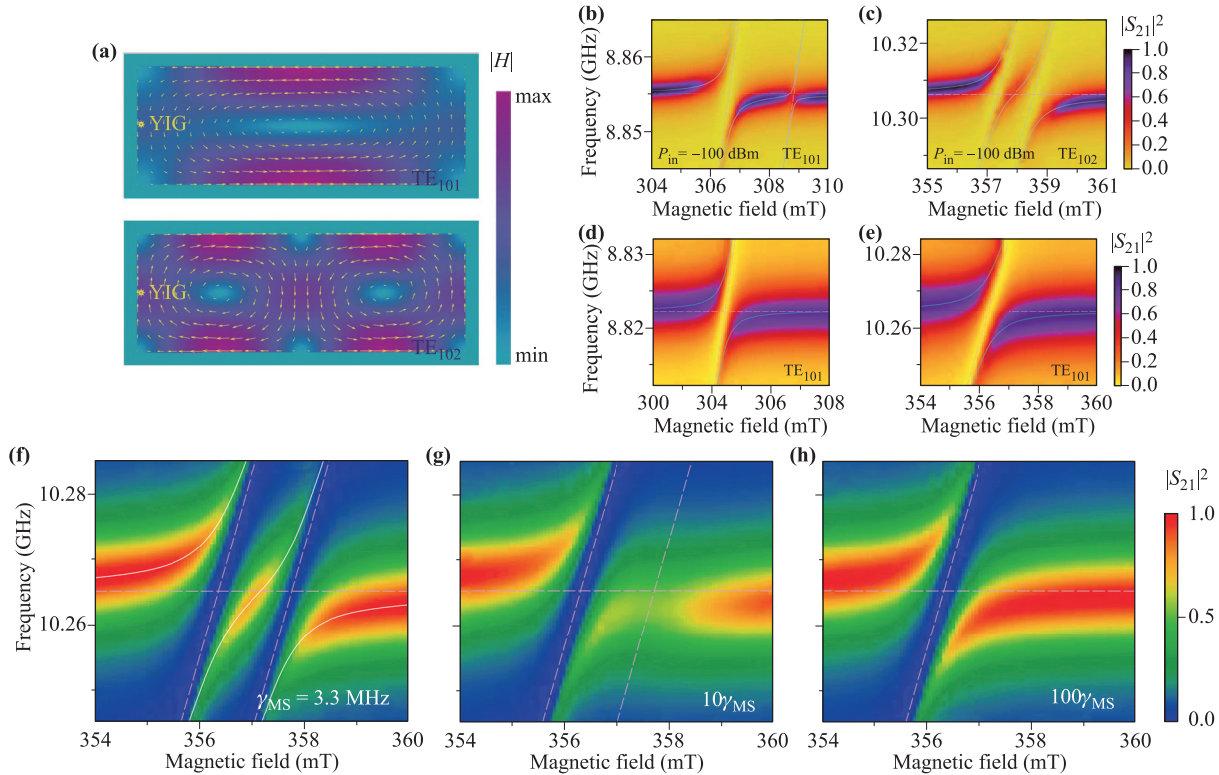

Fig. 3 Measurement and simulation results of microwave photon–magnon strong coupling under different conditions [62]. **(a)** Simulated magnetic-field distribution of the TE_{101} mode and TE_{102} mode. **(b)** Variation trend of system transmission spectrum with bias magnetic field when magnon is coupled with TE_{101} mode at cryogenic. **(c)** Variation trend of system transmission spectrum with bias magnetic field when magnon is coupled with TE_{102} mode at cryogenic. **(d)** Variation trend of system transmission spectrum with bias magnetic field when magnon is coupled with TE_{101} mode at room temperature. **(e)** Variation trend of system transmission spectrum with bias magnetic field when magnon is coupled with TE_{102} mode at room temperature. **(f–h)** The variation trend of the transmission spectrum of the system under different magnetostatic mode damping rates, for the TE_{102} mode. The magnetostatic mode dissipation rates are (f) $\gamma_{MS} = 3.3$ MHz, (g) $\gamma_{MS} = 33$ MHz and (h) $\gamma_{MS} = 330$ MHz, respectively.
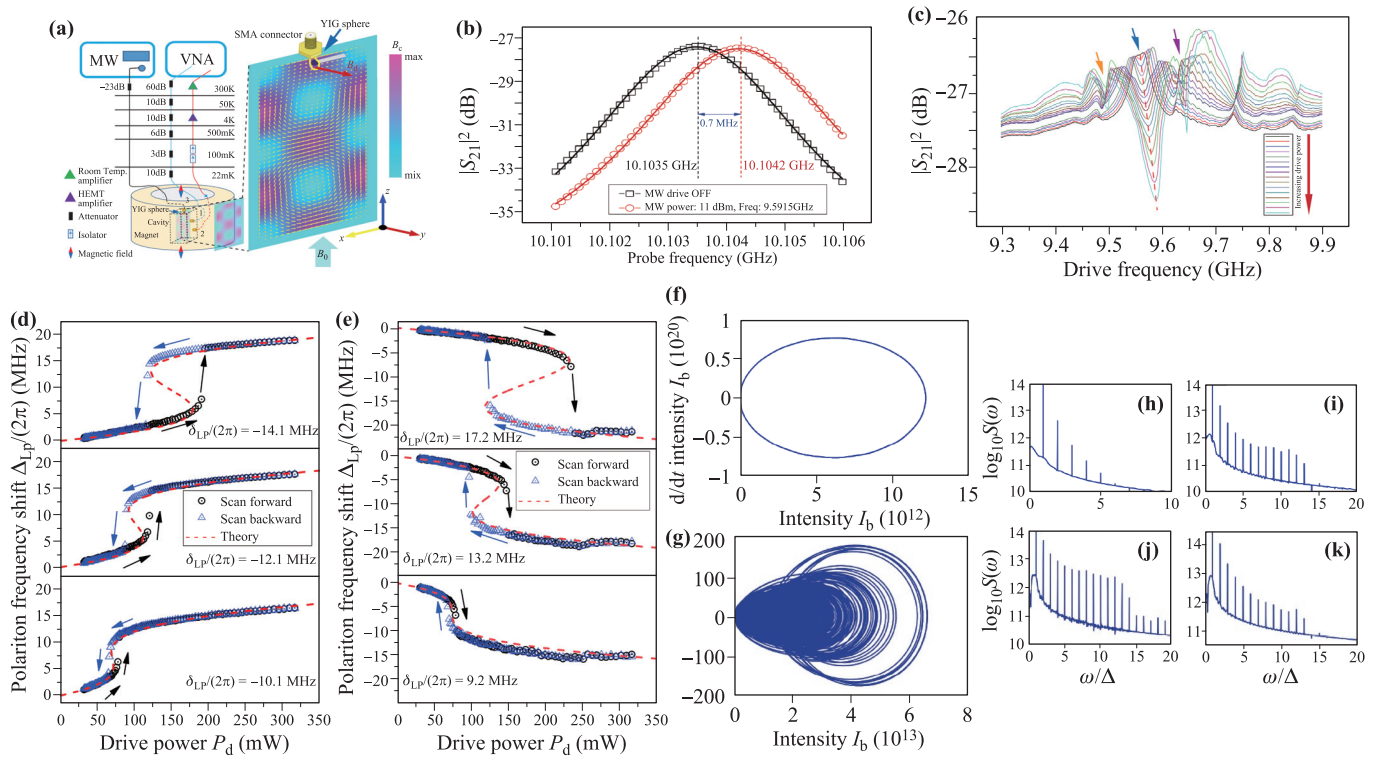
42201-6

Kai Wang, et al., Front. Phys. 17(4), 42201 (2022)

Fig. 4 Magnon-induced nonlinear effects. **(a–c)** Verification of magnon Kerr effect [15]. (a) The left part shows the experimental scheme for realizing the magnon Kerr effect. The right part simulates the magnetic field distribution of the cavity mode TE_{102}. (b) Compare the resonant frequency of the cavity TE_{102} mode when the microwave drive field is turned on and off. (c) With the increase of microwave driving power, the variation trend of the transmission spectrum of the microwave cavity optomagnonical system. The blue arrow represents the Kittel mode and the other two are magnetostatic mode. **(d, e)** Two types of the magnon-polariton bistability [16]. (d) When the [100] crystallographic axis of the YIG sphere is parallel to the bias magnetic field, the measured magnon–polariton bistability. (e) When the [110] crystallographic axis of the YIG sphere is parallel to the bias magnetic field, the measured magnon–polariton bistability. **(f, g)** The phase-space dynamical evolution of the magnons [27]. (f) When the driving field power is 120 mW, the trajectory in the phase space. (g) When the driving field power is 160 mW, the trajectory in the phase space. **(h–k)** Magnon-induced high-order sideband generation under different microwave driving powers P_d [18]. (h) $P_d = 1$ mW. (i) $P_d = 5$ mW. (j) $P_d = 12$ mW. (k) $P_d = 19$ mW.

The simulation result is shown in Figs. 3(f)–(h). They attributed this phenomenon to the change of dissipation. For the MS mode, the dissipation increases sharply as the temperature increases. Meanwhile, the quantum coherence of the MS mode disappears, and the strong coupling between the MS mode and the microwave cavity could not be observed at room temperature. As the FMR mode is robust to the temperature, the dissipation will keep unchanged when the condition changed from cryogenic to room temperature. The strong quantum coherence of the ferromagnetic resonance mode provides an excillent platform for the study of the quantum information transmission and quantum state conversion between different quantum systems.

3.3 Magnon-induced nonlinear effects

The Hamiltonian of the cavity optomagnonical system could be described by Eq. (13). Similarly, by increasing the intensity of the intracavity field, the magnons can

also show nonlinear behaviors. For example, the Kerr-type nonlinearity $K\hat{m}^\dagger\hat{m}\hat{m}^\dagger\hat{m}$ origin from the anisotropy of the magnetocrystalline in the YIG sphere is existed. Here $K = \mu_0 K_{an}\gamma^2/(M_s^2 V_m)$ is the Kerr nonlinear coefficient, where μ_0 denotes the vacuum permeability. K_{an} is the first-order magnetocrystalline anisotropy constant. Compared with the previous results, a contradiction is that the small cavity volume is required to obtain a relatively large nonlinear coefficient, meanwhile the cavity volume is required to be as large as possible to obtain a strong magneto–optical coupling strength. By choosing a YIG sphere with suitable size to couple with a three-dimensional copper cavity, Wang *et al.* observed the magnon Kerr nonlinear effects experimentally [15]. As shown in Fig. 4(a), they applied bias magnetic field parallel to the [100] crystallographic axes of the YIG sphere at cryogenic. In order to generate considerable magnons, the YIG sphere is directly driven by port 3. Due to Kerr nonlinear effect, the cavity frequency and the magnonic frequency are both shifted as shown in Figs. 4(b) and (c).

Subsequently, various studies on the nonlinear effects of magnons have presented, for example, the high-order sidebands generation [18] and chaos generation [27, 28]. In addition, the nonreciprocal transmission of the microwave field can also be realized by using the Kerr nonlinear effect of the magnons [17].

After observing the Kerr nonlinearity of the magnons, Wang *et al.* further observed the bistability of the cavity magnon polaritons in experiment [16]. It is found that the anisotropy are different when applying the magnetic field along different crystal axes of the YIG sphere. This feature leads to the variation of the Kerr nonlinear coefficient. When the applied bias magnetic field is parallel to the [110] crystallographic axes of the YIG sphere, the Kerr nonlinear coefficient is $K = -13\mu_0 K_{an}\gamma^2/(16M_s^2 V_m)$. Obviously, there will be two different bistable behaviors in such a hybrid system, as shown in Figs. 4(d) and (e).

There are also many theoretical studies of the nonlinear effects based on microwave cavity optomagnonics. For example, Wang *et al.* studied the chaotic dynamics of the magnons by using the active cavity-magnon hybrid system, which can realize the conversion from regular motion to chaotic motion [27]. The trajectory of the mode in the phase space is shown in Figs. 4(f), (g). Here Fig. 4(f) shows that the dynamic evolution of the phase space is regular, but when the power of the microwave driving is increased, the trajectory in the phase space becomes completely complex and unpredictable from a regular closed loop, that is, the magnon changes from a periodic oscillation to a chaotic state.

The high-order sideband generation is also considered to be an important nonlinear effect which have potential applications in optical frequency combs and metrology. Recently, Liu *et al.* studied the generation of higher-order sidebands in optomagnon systems directly driven by the microwave field [18]. The high-order sideband generation is tunable by changing the power of the microwave drive field. As shown in Figs. 4(h)–(k), the driving power of the microwave field are 1 mW, 5 mW, 12 mW and 19 mW, respectively. When the power of the microwave driving field is increased, the order and the amplitude of the sidebands both increase. However, when the driving power approaches the threshold, the cut-off order and amplitude of the high-order sidebands are reduced. This can be explained by the change of the Kerr nonlinearity of the magnons. When the power exceeds the threshold, the Kerr nonlinearity intensity no longer increases, but been suppressed. The principles and the effective manipulation of the nonlinear effects in microwave cavity optomagnonics is beneficial to the development of magnetic and optical hybrid devices.

3.4 Construction of non-Hermitian system

In a closed physical system, quantum mechanics requires the operator to be Hermitian to ensure that the eigenvalues are real. In fact, a quantum system will inevitably interact with the surrounding environment to form an open system, and its effective Hamiltonian is usually non-Hermitian. Interestingly, non-Hermitian operators can also have real eigenvalues under a certain Parity–Time (PT) symmetric condition. Furthermore, PT-symmetric systems can be effectively constructed by introducing balanced gain and loss in optical systems, such as the waveguides [65, 66], photonic lattices [67], and optical microcavities [68]. Not an exception, researchers also studied the non-Hermitian properties on optomagnonics. In 2017, Zhang *et al.* studied the exceptional point of cavity magnon–polaritons [19]. They set the gain of the cavity mode equals to the loss rate of the magnons, then a PT-symmetric non-hermitian system could be generated. Here the PT-symmetric Hamiltonian of the designed system could be expressed as:

$$H = (\omega_0 + i\gamma_m)\hat{a}^\dagger\hat{a} + (\omega_0 - i\gamma_m)\hat{m}^\dagger\hat{m} \qquad (16)$$
$$+ g(\hat{a}\hat{m}^\dagger + \hat{a}^\dagger\hat{m}),$$

where the eigenfrequency of the system is $\omega_{1,2} = \omega_0 \pm \sqrt{g^2 - \gamma_m^2}$. Here γ_m is the loss rate of the magnons. The resonance frequency between the cavity mode and the magnons is $\omega_c = \omega_m = \omega_0$. The transition between PT symmetry and symmetry spontaneous breaking can be observed by changing the photon–magnon coupling strength (linearly adjust the position of the YIG sphere).
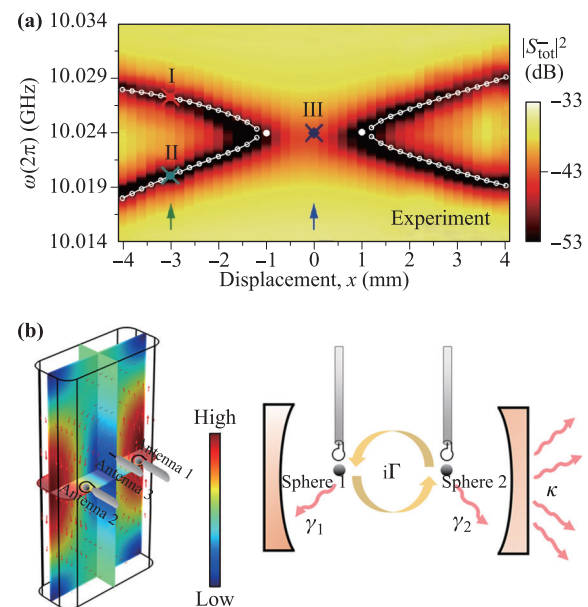

Fig. 5 Construction of non-Hermitian system and observation of exceptional point. **(a)** The relationship between the total output spectrum of the optomagnonical system and the displacement of the YIG sphere in the microwave cavity. By linearly adjusting the position of the YIG sphere, the exceptional point is observed [19]. **(b)** Schematic diagram of the anti-PT symmetric system. The left part simulates the magnetic field distribution of the cavity model TE_{101}. The right part reflects the coupling mechanism of this system [21].

42201-8

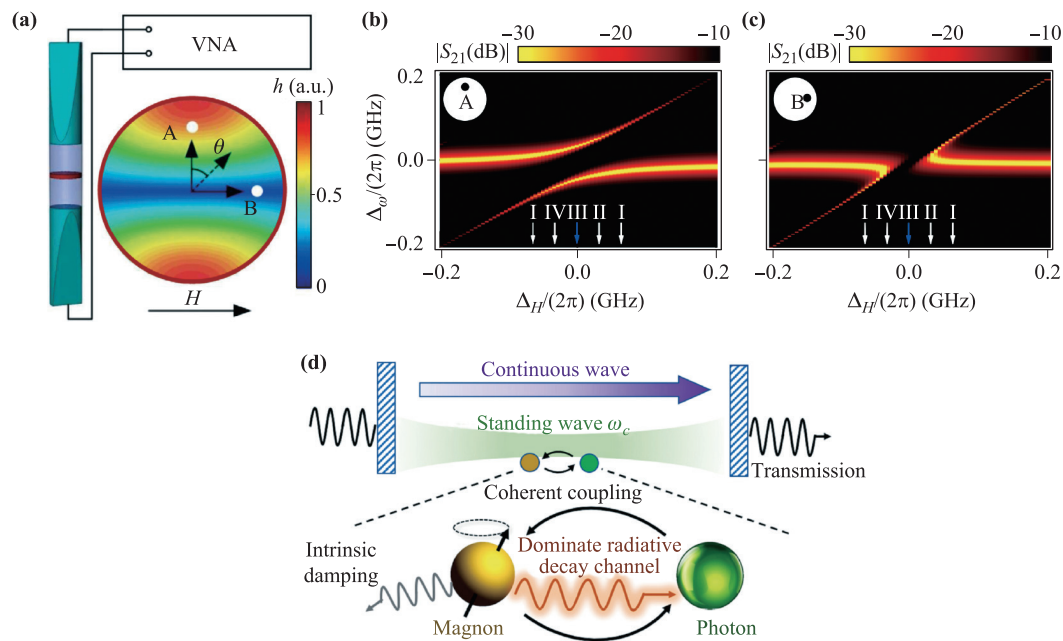Kai Wang, et al., Front. Phys. 17(4), 42201 (2022)

Fig. 6 Dissipative coupling. **(a–c)** Experimental system and measurement results [29]. (a) Schematic diagram of the coupling between the one-dimensional Fabry-Perot-like cavity and the magnon. The right part simulates the magnetic field distribution of TE$_{11}$ mode, which is located in the middle plane of the cavity. Point A indicates that the YIG sphere is located at the antinode, and point B indicates that the YIG sphere is located at the node. (b) The transmission spectrum of the system when the YIG sphere is at point A. (c) The transmission spectrum of the system when the YIG sphere is at point B. **(d)** The microwave cavity supports both standing waves mode and traveling wave mode. When the frequency is detuned (dissipative coupling), the traveling wave mode transfers energy to the environment [35].

As shown in Fig. 5(a), III marks the exceptional-point which is the transition point. Subsequently, Zhang *et al.* used the cavity-magnon hybrid system to experimentally show a three-dimensional exceptional surface in the high-dimensional synthetic space. The research opens a novel way for the high-dimensional manipulation of the non-Hermitian systems [20].

In addition to the PT-symmetric system, the anti-Parity–Time (APT) symmetric system is also proposed as another non-Hermitian system. It is conjugate to the properties observed in the PT symmetric system. And mathematically, the Hamiltonian of these two systems has the following relationship: $H^{(\mathrm{APT})} = \pm iH^{(\mathrm{PT})}$ [69, 70]. Recently, Zhao *et al.* constructed an APT-symmetric system using a cavity optomagnonic system [21]. They directly measured the energy transmission spectra from the magnon with coupling-loop technique, and the results are shown in Fig. 5(b). Different from the mode anti-crossing in the strong coupling scheme, the APT-symmetry shows the mode attraction at the phase transition point. These studies have enriched the understanding of non-Hermitian magnon systems and also demonstrated the advantages of the photon–magnon coupling system.

3.5 Dissipative coupling

The strong photon–magnon interaction is the key element of the implementation of quantum information processing.

Here in the cavity-optomagnonical system, the photon–magnon coupling relies mainly on the dipole-dipole interaction. Recently, a special approach of photon–magnon dissipative coupling has been discovered by Harder *et al.* [29]. By placing a YIG sphere in the 1D Fabry–Perot-like cavity as shown in Fig. 6(a), they compared the spectrum in the anti-node and the node of the cavity mode. The cavity is composed of two connected circular–rectangular transition waveguides, and the TE$_{11}$ mode with 13.205 GHz frequency is located in the middle plane of the cavity. When the YIG sphere is placed on the antinode of the cavity field, the anti-crossing of the photon–magnon mode could be observed. When the YIG sphere is located at the node of the cavity magnetic field, the photon–magnon mode attraction could be observed. The results are shown in Fig. 6(c), and they attributed this kind of mode attraction to the cavity Lenz effect. In the presence of both the coherent coupling and the dissipative coupling, the interaction Hamiltonian between magnon and microwave photons can be written as

$$H/\hbar = \omega_c \hat{a}^\dagger \hat{a} + \omega_m \hat{m}^\dagger \hat{m} + g(\hat{a}^\dagger \hat{m} + e^{i\Phi} \hat{m}^\dagger \hat{a}), \quad (17)$$

where the phase Φ describes the competitive effect between the coherent coupling and the dissipative coupling. Obviously, when Φ is zero, it becomes coherent coupling.

In the previous experiments, the dissipative coupling was classically explained as the cavity Lenz effect, but its microscopic principle is still unclear. As shown in

Kai Wang, et al., Front. Phys. 17(4), 42201 (2022)

42201-9

Fig. 6(d), Yao *et al.* used a microwave cavity that supports both standing waves and traveling waves to couple with the magnons [35]. Their results show that the traveling wave is the origin of the dissipative coupling. Yu *et al.* proposed an effective three-oscillator coupled model to explain the mechanism of the dissipative coupling [34]. Here in this model, the magnons and microwave photons interact with a common third oscillator through the dissipation channel, where the third oscillator can be considered as an invisible cavity mode with larger dissipation. This model is not limited to microwave cavity optomagnonical systems, and is expected to further applied in designing the generalized dissipative coupling systems.

Meanwhile, the researchers are also exploring the applications of the dispersion coupling. Wang *et al.* took the advantages of the cooperative effect of both the coherent coupling and the dissipative coupling in optomagnonical system, and realized non-reciprocal microwave transmission [33]. Yuan *et al.* found that PT symmetry can be spontaneously broken when the photon–magnon mode attraction occures [71] and the magnons and photons can form a high-fidelity Bell state in this region. This indirects that the coupling mechanism could be widely applied in open cavity systems, which provides new ideas for constructing hybrid quantum systems.

3.6 Slow light

Slow light effect is an important optical phenomenon and a key process in information storage and processing [72–76], which also provides a solution for quantum storage [77–80]. Meanwhile, slow light in microwave cavity optomagnonical system also exhibits important physical significance. Liu *et al.* first theoretically studied the slow light effect in the cavity magnon–photon system [81], and the slow light effect could be observed at room temperature. The group velocity delay is also tunable by the external magnetic field. In addition, the conversion between fast light and slow light can be achieved by tuning the magnon–photon coupling strength. Subsequently, Liu *et al.* theoretically studied the slow light in the cascaded magnon–photon system [82]. Compared with the single cavity system, when two identical microwave optomagnonic cavities are cascaded, the group delay becomes smaller. Their result shows that the simple cascade have no benefit for obvious slow light effect. However, the group delay will increase significantly when changing the relative length of the microcavities.

Recently, Zhao *et al.* studied the phase-controlled transmission properties in the microwave optomagnonical system [83] and the experimental setup is shown in Fig. 7(a). Considering the relative phase and amplitude of the magnon pump and cavity probe, the Hamiltonian of the system could be expressed as ($\hbar = 1$)

$$H = \omega_c \hat{a}^\dagger \hat{a} + \omega_m \hat{m}^\dagger \hat{m} + g(\hat{a}^\dagger \hat{m} + \hat{m}^\dagger \hat{a})$$

$$+ i\sqrt{2\eta_c \kappa_c} \varepsilon_c (\hat{a}^\dagger e^{-i\omega_p t} - \hat{a} e^{i\omega_p t})$$
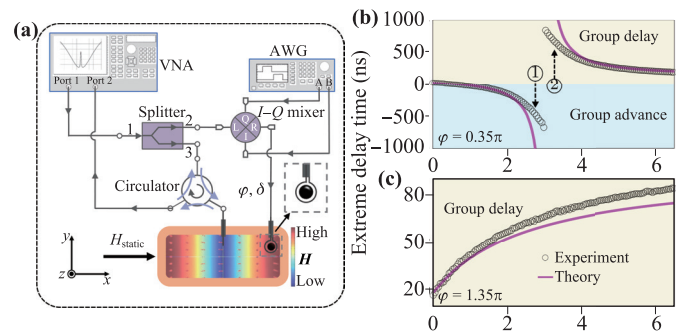

Fig. 7 Slow light generation in the microwave cavity [83]. **(a)** Experimental setup for slow light generation. The magnetic field distribution of TE_{101} mode is simulated in the lower part. **(b, c)** Group velocity delay measurement results.

$$+ i\sqrt{2\eta_m \kappa_m} \varepsilon_m (\hat{m}^\dagger e^{-i\omega_p t - i\phi} - \hat{m} e^{i\omega_p t + i\phi}), \quad (18)$$

where ε_c and ε_m are the microwave amplitude of the driving cavity and magnon, respectively. ω_p denotes the probe frequency, and η_c (η_m) is the coupling parameter of the cavity (magnon). As shown in Figs. 7(b) and (c), the group delay has different performance of changing as the variation of the phase and the amplitude ratios.

3.7 Electrical detection method of microwave photon–magnon coupling

The strength of magneto–optical interaction can be characterized by analyzing the reflection spectrum and transmission spectrum using the vector network analyzer. However, it can also be readout by using the electrical detection based on the spin pumping effect [84]. Bai *et al.* designed an electrical detection experiment [85], as shown in Fig. 8(a). Different from the method using vector network analyzer, the system is driven by microwave photons with fixed frequency, then the electrical signals of the spin current is measured under magnetic field scanning. These two methods could both be used to measure the optomagnonic system, and the results are shown in Figs. 8(b) and (c). It is obvious that in Fig. 8(c), the inflection point at the cavity resonance frequency symbols the coupling between microwave photon and magnon.

In the following works, they realized the long-distance manipulation of spin current [86]. As shown in Fig. 8(d), two YIG/Pt samples are placed in different positions of the same microwave resonator. When the angle θ between the local microwave magnetic field of one of the samples and the external magnetic field changes, the spin current also changed accordingly. Even more, they found that the spin current in another sample also change, but the trend is opposite. The electrical detection method combines cavity quantum electrodynamics with the spin electronics, which provides a novel method for spin currents manipulation, and promotes the development of cavity spintronic devices.
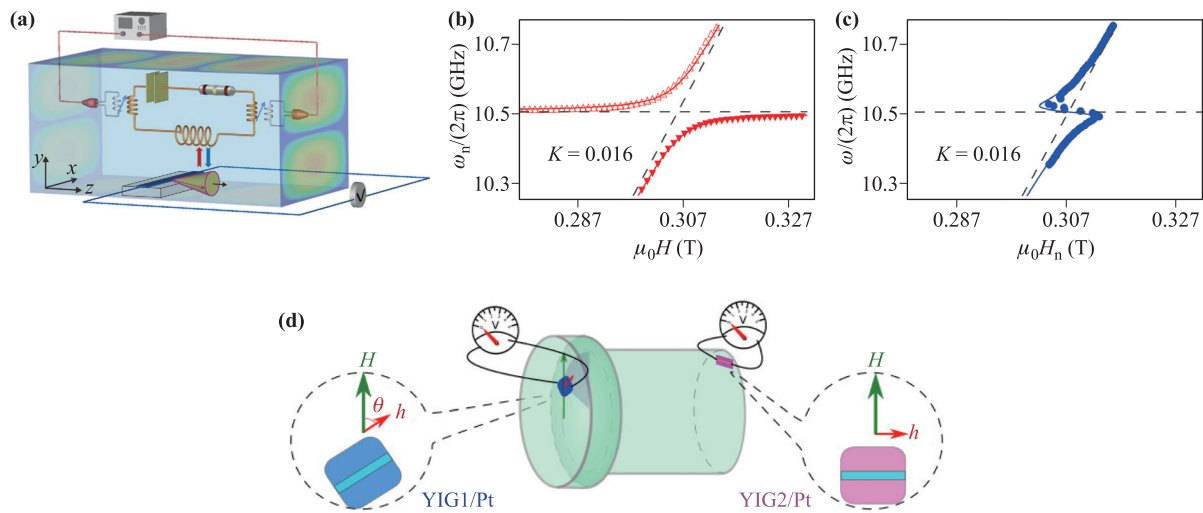
42201-10

Kai Wang, et al., Front. Phys. 17(4), 42201 (2022)

Fig. 8 Electrical detection method. **(a)** Schematic diagram of the experimental device. The microwave cavity is equivalent to an RLC circuit. **(b)** Measurement results obtained by using a vector network analyzer to measure the transmission spectrum of the system. **(c)** Measurement results obtained by electrical testing methods [85]. **(d)** Experimental scheme for long-distance manipulation of spin currents [86].

3.8 Entanglement and squeezed state generation

Entangled and squeezed states are important resources for quantum precision measurement and quantum communications, and the realization of the preparation of entangled and squeezed states in macroscopic systems is of great significance in quantum information science. For example, the photon–phonon entanglement [87–90] and the mechanical squeezed state [91, 92] have been studied in cavity optomechanical systems. Cavity optomagnical system is also a macroscopic quantum system which can be engineered in a similarly way. Li *et al.* demonstrated the generation of the triple entanglement of magnons, microwave photons and phonons in the cavity magnomechanics system [93]. The entanglement origins from magnetostrictive interaction of magnons and phonons in the scheme. Without introducing magnon–phonon interaction, Yang *et al.* theoretically proved that the Kerr nonlinearity of the magnons is reliable for enhancing the entanglement [94]. They illustrated that two microwave cavity modes could be coupled to a common magnon mode. And then, the photon–photon entanglement, the photon–magnon entanglement and the photon–magnon–photon entanglement all can be enhanced by the magnonic Kerr nonlinear effect. Compared with the cavity optomechanical system, the entanglement is robust to temperature for cavity optomagnonics.

In the study of magnon squeezing, Li *et al.* theoretically proved the existence of the magnon squeezed state. Even more, they find the magnon squeezed state can be transferred to the phonon through the magnetostrictive effect [95]. In their scheme, a weak squeeze vacuum field is used to drive the cavity, then photon and magnon squeezed state can be transferred into each other. Subsequently, Zhang *et al.* realized the magnon squeezed state

by applying the two-tone microwave fields to drive the magnon mode in the cavity magnomechanics system [96]. The magnons squeezed state can also be transferred to the photons through the photon–magnon interaction. And we believe that the photon–magnon interaction provides a promising way to explore the quantum–classical boundary which is also opening up a new path for quantum information processing.

4 Optical cavity-optomagnonics

In this section, we will introduce the phenomena caused by the photon–magnon coupling in the optical cavities. Different from the photon–magnon coupling in the microwave frequency range, the frequency matching condition is not satisfied due to the high optical frequency, then the magnetic dipole interaction between the optical photons and the magnons could be suppressed. The corresponding coupling dynamics relies on the Faraday effect, when light propagates in the magnetic material, the polarization direction of the light will be changed. The key issue is how to effectively couple the electromagnetic field of the optical frequency with the YIG microsphere. Fortunately, high-efficient fiber taper coupling provides the an efficient way of optical pumping of the nanostructure such as the optical microcavity. Due to the mismatch between the refractive index of the YIG sphere and the silica fiber, the coupling between the two systems is difficult. To overcome this issue, Osada *et al.* studied the efficient coupling between a fiber taper and the YIG sphere, and excited the whispering gallery mode in the magnetic sphere [7]. Another method is to couple light using prisms, the high refractive index rutile prism can couple the optical frequency electromagnetic field into the YIG sphere [8]. Because of

Kai Wang, et al., Front. Phys. 17(4), 42201 (2022)

42201-11

the birefringence effect in the rutile prism, this method is conducive to the realization of polarization-dependent experimental schemes. In addition, Zhang *et al.* used the silicon nitride integrated optical waveguide to effectively couple the telecommunication C-band light into the YIG microsphere [9]. These methods enable the coherent manipulation of magnons in solid-state systems, which also promotes the development of optical cavity optomagnonics.

4.1 Whispering gallery mode in magnetic materials

YIG materials have low absorption loss at infrared wavelengths, and it is feasible to directly use the YIG spheres as the high quality factor optical whispering gallery mode microcavities. The most commonly used coupling methods are fiber tapers, prisms, and silicon nitride waveguides, as shown in Figs. 9(a)–(c). All these schemes have realized the Brillouin scattering induced by the magnons. From the interaction Hamiltonian Eq. (11), we conclude the dynamics that the annihilation of a TM polarized photon and a magnon will produce a TE polarized photon, and vice versa. Kosminski *et al.* described the spin–light coupling theory in cavity optomagnonics [50]. When light propagates on the surface of the YIG sphere, the photons and the magnons can be coupled through the Faraday effect. Based on the model shown in Fig. 9(d), the spin precession frequency is Ω, and the magnetization is along the z-axis. Assuming that the circularly polarized optical modes is only coupled to the x component of the spin (S_x), the Hamiltonian of the system in the rotating frame of the laser frequency ω_L can be written as

$$\hat{H}/\hbar = -\Delta \hat{a}^\dagger \hat{a} - \Omega \hat{S}_z + G \hat{S}_x \hat{a}^\dagger \hat{a}, \qquad (19)$$

where, $\hat{a}^\dagger$ and $\hat{a}$ are the creation operator and annihilation operator of the optical-photons, respectively. And $\Delta = \omega_L - \omega_{cavity}$ denotes the detuning. When the nonlinearity of the system is considered, the system would enter chaos region when the dissipation is lower than the threshold.

The photon–magnon coupling strength in the optical cavity is weak as the overlap of the modes between the Kittel mode and the optical whispering gallery mode is very small. So it is difficult to observe the nonlinear effect in experiment. To enhance the photon–magnon coupling strength, the researchers proposed to use high-order magnons to couple with the photons [40–43]. According to the results, several high-order magnon modes are concentrated on the surface of the YIG sphere, which improves the spatial overlap with the photon mode and would increase the coupling strength. Figure 9(e) shows the transverse magnetization distribution of Kittel mode and the related high-order magnetic modes. Meanwhile, an important issue to be addressed is the generation and identification of the higher-order magnon modes. To meet this requirement, Gloppe *et al.* studied the structural imaging of the magnetostatic modes in ferromagnetic microspheres [43]. Haigh *et al.* experimentally proved that the coupling strength between the non-uniform magnetized high-order magnons and photons is higher, and experimentally verified the optical scattering produced by high-order magnon modes [42]. The magnetostatic mode in the ferromagnetic sphere is also called the Walker mode, which has both the orbital angular momentum and the spin angular momentum. It provides more degrees of freedom for the hybrid system. Osada *et al.* observed that the Brillouin light scattering has different irreversible behaviors in ferromagnetic spheres [41]. They attributed this phenomenon to the coupling between the orbital an-
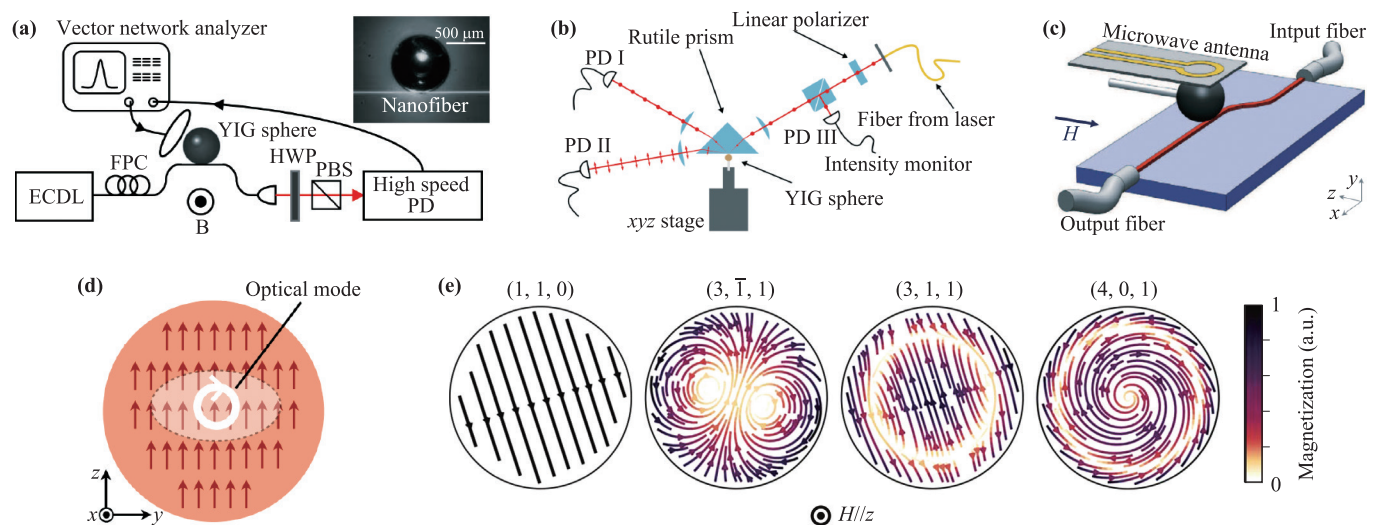

Fig. 9 Optical cavity optomagnonical system. **(a)** Optical fiber taper coupling measurement system [7]. **(b)** Prism coupling measurement system [8]. **(c)** Waveguide coupling measurement system [9]. **(d)** The schematic diagram of an optomagnonic cavity. The magnetization direction is along the *z*-axis, and the magnons are coupled to the circularly polarized optical mode [50]. **(e)** Kittel mode and some high-order magnetic modes [40].

42201-12

Kai Wang, et al., Front. Phys. 17(4), 42201 (2022)

gular momentum of the Walker mode magnons and the whispering gallery mode photons. Different from Walker modes existing in spheres, Damon–Eshbach (DE) modes correspond to the surface spin waves and distributed on the surface of the medium [97, 98]. Sharma *et al.* theoretically demonstrated that Brillouin light scattering can be enhanced for DE magnon modes with large angular momentum [11]. Moreover, the mode overlap can also be increased by designing the suitable micro-nano structure of the optomagnonic cavity [13, 44, 99]. Compared with the sphere cavity, the volume of the spin wave mode in the disk is relatively small which can increase the coupling strength between the photons and the magnons. Graf *et al.* theoretically studied the coupling between the magnetic vortex and the photons in a microdisk cavity [44]. Graf *et al.* theoretically simulated an optomagnonic crystal cavity [99]. By designing the period and size of the air hole, the optical photon–magnon coupling strength in the kHz range can be obtained.

4.2 Cavity-optomagnonics hybrid quantum systems

The optical microcavity can greatly enhance the interaction between the light field and solid system, which is of great significance to the further study of dynamical behaviors and manipulation of the quantum system. The light–atom interaction and photon–phonon interaction have been realized in cavity quantum electrodynamics and cavity optomechanics systems. However, single interaction leads to fewer tunable parameters, which limits the flexibility of the system. Therefore, several current works turn to the study of hybrid quantum systems. Recently, the emerge of optomagnonics makes it possible to achieve the quantum magneto–optical regulation. Liu *et al.* theoretically demonstrated the effective coupling enhancement under the pump–probe scheme [100], and observed the electromagnetically induced transparency effect and the Purcell effect. Gao *et al.* studied the interaction between the phonons and magnons in the YIG sphere, and explained the principle that the phonon and magnon modes are connected through optical mediation in the hybrid system [101]. In addition, the topological features of this hybrid system are also discussed.

In the context of non-classical states generation, there is a significant progress based on cavity optomagnonics. Bittencourt *et al.* proposed a magnon heralding protocol to generate the magnon Fock states in cavity optomagnonics [102], the results are shown in Fig. 10(a). By linearizing the Hamiltonian and considering the selection rules, the optomagnonics Hamiltonian can be written as

$$\hat{H} = \hbar G_{12}^- \hat{m}^\dagger e^{i\Omega t}(\alpha_1^* \hat{a}_2 e^{i\Delta_2 t} + \alpha_2 \hat{a}_1^\dagger e^{-i\Delta_1 t}) + H.C.. \quad (20)$$

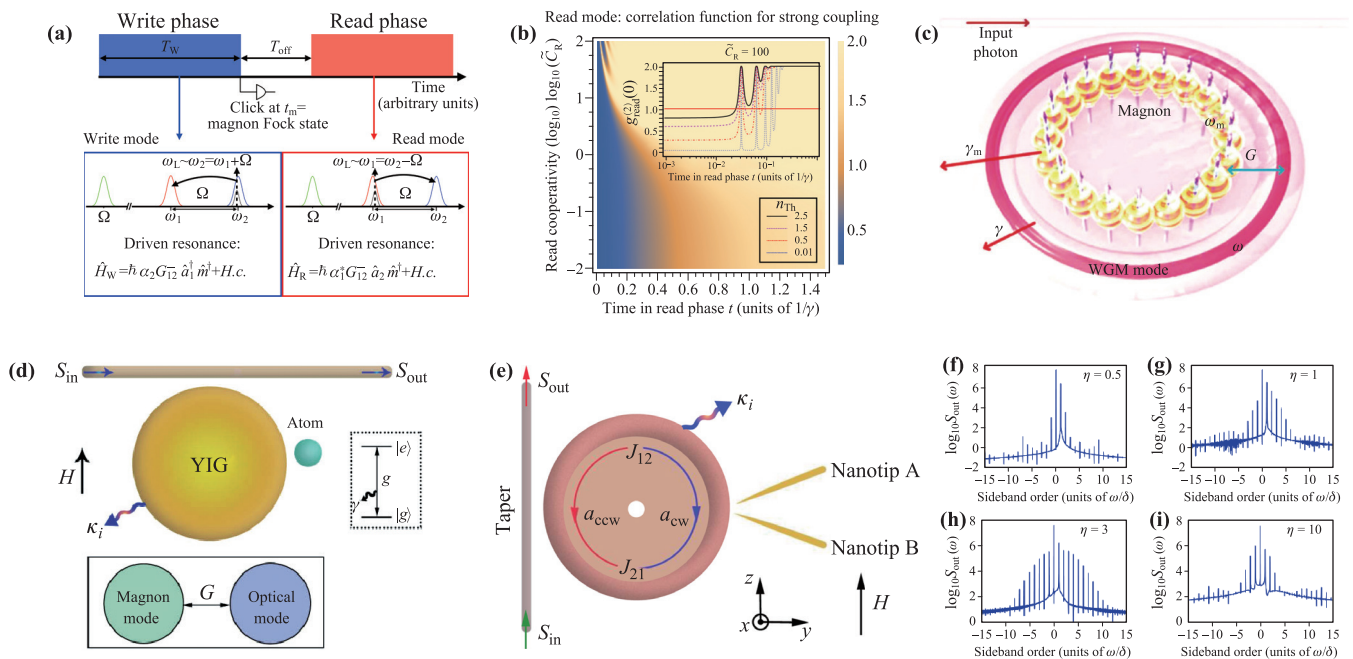Here $\hat{a}_1$ $\hat{a}_2$ $(\hat{a}_1^\dagger$ $\hat{a}_2^\dagger)$ represents the annihilation (creation)

Fig. 10 Hybrid quantum systems. **(a, b)** Magnon-heralding protocol [102]. (a) Description of the "write" and "read" scheme. (b) The second-order correlation function of the "read" scheme in the strong coupling regime which is used to detect the generation of magnon heralding states. **(c)** A theoretical model describes the coupling between optical photon and magnon [51]. **(d)** Schematic diagram of the hybrid atom-cavity optomagnonical system [55]. **(e–i)** The cavity optomagnonical system with two nanotips [54]. (e) Schematic diagram of the hybrid quantum system. Two nanotips are used to induce asymmetric scattering of optical modes. η is related to the spin precession frequency. (f) $\eta = 0.5$, (g) $\eta = 1$, (h) $\eta = 3$, and (i) $\eta = 10$. High-order sideband generation is closely related to the frequency of the spin precession.

operator of photon mode 1 and photon mode 2, respectively. Ω is the frequency of the magnons. Δ_i $(i = 1, 2)$ are the detunings between the laser frequency ω_L and the frequency of the mode i ω_i. G_{12}^- $((G_{12}^-)^* = G_{21}^+)$ denotes the coupling strength of photon–magnon interaction, which is related to the Faraday rotation angle θ_F. α_i is the steady-state values of mode i. By randomly choosing the pump mode-1 or mode-2, the optomagnonics Hamiltonian Eq. (20) can be divided into "write" and "read" Hamiltonian as

$$\hat{H}_{write} = \hbar(\alpha_2^* G_{21}^+ \hat{a}_1 \hat{m} + \alpha_2 G_{12}^- \hat{a}_1^\dagger \hat{m}^\dagger), \tag{21}$$

$$\hat{H}_{red} = \hbar(\alpha_1^* G_{12}^- \hat{a}_2 \hat{m}^\dagger + \alpha_1 G_{21}^+ \hat{a}_2^\dagger \hat{m}). \tag{22}$$

When choosing the pumping mode 2 ($\alpha_1 = 0$), the system is direct to the "write" Hamiltonian; while choosing the pumping mode 1 ($\alpha_2 = 0$), the system is direct to the "read" Hamiltonian. This protocol is sensitive to the initial state of the magnons and requires an initial state close to the vacuum state. After the preparation of the initial state, the related photon–magnon pair is generated through the "write" interaction. Then, the magnon Fock state could be generated by measuring the "write" photon state. Finally, it could be read out by the "read" interaction. In addition, it is also demonstrated that the quantum properties of the system can be decided by measuring the second-order correlation of Mode-2. The photon–magnon can be converted coherently under the strong photon–magnon coupling, and the Rabi oscillation characteristics is shown in Fig. 10(b). Later, Gao et $al.$ studied the photon blockade effect of the supermode photons in the cavity optomagnonical system and analyzed the correlation functions of different orders [52]. The realization of photon blockade effect is beneficial to the preparation of single photon source with high quality.

Similar to the microwave cavity, the photon–magnon interaction can also be used to tune the nonlinear effects [51, 53–55]. In 2020, Gao et $al.$ discovered the chaotic phenomenon of photonic superposed states in an optomagnonical cavity [51]. The model of the system is shown in Fig. 10(c). The chaotic behavior of the system can be observed by tuning the photon–magnon coupling strength and the dissipation. Later, Xu et $al.$ introduced the optomagnonics in an optical PT symmetric system [53]. The proposed system consists of a YIG dissipative sphere cavity and a doped gain sphere cavity. It is found that the size of the spin component influences the dynamics of the system. By tuning the external bias magnetic field, the chaotic behavior of the system can be manipulated. Subsequently, they studied the generation of higher-order sidebands in the optomagnonical hybrid quantum systems [55]. Fig. 10(d) shows the hybrid atom-cavity optomagnonical system, photons are coupled with the magnons and two-level atoms in the system. Combined with the input–output relationship $s_{out}(t) = s_{in}(t) - \sqrt{2\kappa}a(t)$ and the Fourier transformation, the spectral change of the output light field can be expressed as

$$S(\omega) \propto \left| \int_{-\infty}^{\infty} s_{out}(t) e^{-i\omega t} \, dt \right|. \tag{23}$$

They found that the generation of high-order sidebands are related to the coupling strength between the atoms and the cavity photons, the component of the magnons S_x and the dissipation of the cavity. By tuning these parameters, the modulation of the sidebands can be realized. Figure. 10(e) is the schematic diagram of another optomagnonical hybrid quantum system [54]. The YIG microresonator is coupled with two silica nanotips, which are placed in the evanescent field of the cavity. The optical mode is asymmetrically scatted by tuning the relative angle of the two nanotips , the exceptional points (Eps) in the non-Hermitian system could appear periodically. They found that in the non-EP case, the order and amplitude of the sidebands are both enhanced. In particular, the sideband spectrum changes with the spin precession frequency, as shown in Figs. 10(f)–(i). The sideband modulation can also be performed by tuning the external magnetic field. Obviously, the introduction of photon–magnon interaction enriches the structure of the hybrid quantum systems, and has unique advantages when constructing the quantum information processing scheme.

4.3 Other types of optomagnonic cavities

In addition to magneto–optical whispering gallery mode resonators, there are several other types of optomagnonic cavities, such as the planar optomagnonic cavities [46–49] and the waveguide cavities [13]. Pantazopoulos et $al.$ carried out a series of studies on planar optomagnonic cavities. The system consists of two dielectric Bragg mirrors and a magnetic garnet film, forming a single optomagnonic cavity with a sandwich structure [46] as shown in Fig. 11(a). The work shows the photon–magnon strong coupling that can be achieved in the planar optomagnonic cavity. After that, they also described the optical spin wave interaction in a planar optomagnonic cavity under the full dynamic time Floquet scattering matrix method with arbitrary order accuracy [47]. Further, they extended this method to stratified media subject to a periodic spatiotemporal modulation [48].

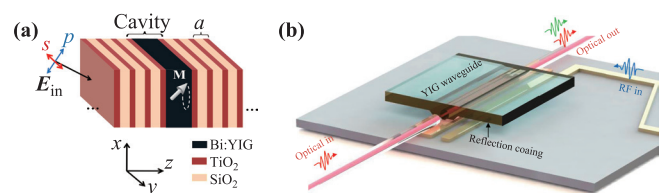The waveguide cavity can also be used to construct the

Fig. 11 Optomagnonic cavities. **(a)** Schematic diagram of a planar optomagnonic cavities [46]. **(b)** Schematic diagram of the optomagnonic waveguide cavity [13].

42201-14

Kai Wang, et al., Front. Phys. 17(4), 42201 (2022)

optomagnonical system. Zhu *et al.* designed a cavity optomagnonic device based on the integrated waveguide [13] as shown in Fig. 11(b). The system consists of YIG rib waveguide and rf microstrip cavity. The microwave resonator is placed under the YIG waveguide to effectively coupling the magnons. When the triple-resonance condition is satisfied, the microwave–optical photon conversion could be realized. In fact, these two cavities belong to the Fabry–Perot cavity in essence. It is found that the photon–magnon mode overlap can be increased by changing the structure design. In a word, these research enriches the applications of the integrate optomagnonic devices.

5   Summary

Here in this review, we discussed the magnon–photon interaction in ferromagnetic materials both in microwave frequency and the optical frequency cavity optomagnonical system. In the microwave cavity, photons and magnons can achieve strong and ultrastrong coupling which is usually experimentally detected by the anti-crossing transmission spectrum of the system through the vector network analyzer. On the other hand, the electrical detection method is also of great significance, which can be combined with spintronics, and is expected to realize spin current information processing [103–107]. Based on the strong coupling, the studies on nonlinear effects and non-Hermitian systems are rapidly emerged. Soon afterwards, a new coupling mechanism was discovered, namely the dissipative coupling. These research promotes the development of non-reciprocal quantum devices [17, 33, 108, 109]. Moreover, the microwave cavity optomagnonical system has important applications in dark matter search [110]. Simultaneously, the research on the quantum manipulation of magnon is also ongoing. Theoretically, the proposals to realize the magnon squeezed state and magnon entanglement have been proposed [93–96, 111, 112], and the scheme to realize the spin cat state has also been proposed [113].

In an optical cavity, the coupling between the optical photons and the magnons relies on the Faraday effect. Here we discussed the methods to excite the optical whispering gallery modes of the YIG sphere. On the-state-of-the-art, the coupling strength between optical photons and magnons is still weak. Fortunately, this issue can be solved by coupling high-order magnon modes or designing new micro–nano structures. Profit from the advanced manufacturing technology, the preparation of optomagnonics cavity has enough space for optimization. In the process of optimization, waveguide cavities and planar optomagnonic cavities have been used which can also be integrated. Moreover, the coherent conversion between optical photons and magnons is of great significance. Combined with the superconducting system, the magnons and superconducting qubits can be coupled with each other [114]. Then, through the interaction between the optical photons and magnons, long-distance transmission of qubits can be realized, which greatly compensates for the shortcomings of superconducting systems. Therefore, the cavity optomagnonical system is expected to realize a high-efficiency quantum interface. In summary, the cavity optomagnonics promotes the development of hybrid quantum systems and also provides a novel platform for the study of macroscopic quantum phenomena.

References

1. R. L. Stamps, S. Breitkreutz, J. Åkerman, A. V. Chumak, Y. C. Otani, G. E. W. Bauer, J. U. Thiele, M. Bowen, S. A. Majetich, M. Kläui, I. L. Prejbeanu, B. Dieny, N. M. Dempsey, and B. Hillebrands, The 2014 magnetism roadmap, *J. Phys. D: Appl. Phys.* 47, 333001 (2014)

2. Ö. O. Soykal and M. E. Flatté, Strong field interactions between a nanomagnet and a photonic cavity, *Phys. Rev. Lett.* 104, 077202 (2010)

3. Ö. O. Soykal and M. E. Flatté, Size dependence of strong coupling between nanomagnets and photonic cavities, *Phys. Rev. B* 82, 104413 (2010)

4. H. Huebl, C. W. Zollitsch, J. Lotze, F. Hocke, M. Greifenstein, A. Marx, R. Gross, and S. T. B. Goennenwein, Strong field interactions between a nanomagnet and a photonic cavity, *Phys. Rev. Lett.* 111, 127003 (2013)

5. Y. Tabuchi, S. Ishino, T. Ishikawa, R. Yamazaki, K. Usami, and Y. Nakamura, Hybridizing Ferromagnetic Magnons and microwave photons in the quantum limit, *Phys. Rev. Lett.* 113, 083603 (2014)

6. X. Zhang, C. Zou, L. Jiang, and H. X. Tang, Strongly coupled magnons and cavity microwave photons, *Phys. Rev. Lett.* 113, 156401 (2014)

7. A. Osada, R. Hisatomi, A. Noguchi, Y. Tabuchi, R. Yamazaki, K. Usami, M. Sadgrove, R. Yalla, M. Nomura, and Y. Nakamura, Cavity optomagnonics with spin–orbit coupled photons, *Phys. Rev. Lett.* 116, 223601 (2016)

Kai Wang, et al., Front. Phys. 17(4), 42201 (2022)

42201-15

8. J. A. Haigh, S. Langenfeld, N. J. Lambert, J. J. Baumberg, A. J. Ramsay, A. Nunnenkamp, and A. J. Ferguson, Magneto–optical coupling in whispering-gallery-mode resonators, *Phys. Rev. A* 92, 063845 (2015)

9. X. Zhang, N. Zhu, C.-L. Zou, and H. X. Tang, Optomagnonic whispering gallery microresonators, *Phys. Rev. Lett.* 117, 123605 (2016)

10. J. A. Haigh, A. Nunnenkamp, A. J. Ramsay, and A. J. Ferguson, Triple-resonant brillouin light scattering in Magneto–optical cavities, *Phys. Rev. Lett.* 117, 133602 (2016)

11. S. Sharma, Y. M. Blanter, and G. E. W. Bauer, Light scattering by magnons in whispering gallery mode cavities, *Phys. Rev. B* 96, 094412 (2017)

12. R. Hisatomi, A. Osada, Y. Tabuchi, T. Ishikawa, A. Noguchi, R. Yamazaki, K. Usami, and Y. Nakamura, Bidirectional conversion between microwave and light via ferromagnetic magnons, *Phys. Rev. B* 93, 174427 (2016)

13. N. Zhu, X. Zhang, X. Han, C.-L. Zou, C. Zhong, C.-H. Wang, L. Jiang, and H. X. Tang, Waveguide cavity optomagnonics for microwave-to-optics conversion, *Optica* 7(10), 1291 (2020)

14. Y. S. Ihn, S.-Y. Lee, D. Kim, S. Hyuk Yim, and Z. Kim, Coherent multimode conversion from microwave to optical wave via a magnon-cavity hybrid system, *Phys. Rev. B* 102, 064418 (2020)

15. Y.-P. Wang, G.-Q. Zhang, D. Zhang, X.-Q. Luo, W. Xiong, S.-P. Wang, T.-F. Li, C.-M. Hu, and J. Q. You, Magnon Kerr effect in a strongly coupled cavity-magnon system, *Phys. Rev. B* 94, 224410 (2016)

16. Y.-P. Wang, G.-Q. Zhang, D. Zhang, T.-F. Li, C.-M. Hu, and J. Q. You, Bistability of cavity magnon polaritons, *Phys. Rev. Lett.* 120, 057202 (2018)

17. C. Kong, H. Xiong, and Y. Wu, Magnon-induced nonreciprocity based on the magnon kerr effect, *Phys. Rev. Appl.* 12, 034001 (2019)

18. Z.-X. Liu, B. Wang, H. Xiong, and Y. Wu, Magnon-induced high-order sideband generation, *Opt. Lett.* 43, 3698 (2018)

19. D. Zhang, X.-Q. Luo, Y.-P. Wang, T.-F. Li, and J. Q. You, Observation of the exceptional point in cavity magnon-polaritons, *Nat. Commun.* 8, 1368 (2017)

20. G.-Q. Zhang and J. Q. You, Higher-order exceptional point in a cavity magnonics system, *Phys. Rev. B* 99, 054404 (2019)

21. J. Zhao, Y. Liu, L. Wu, C.-K. Duan, Y.-X. Liu, and J. Du, Observation of anti-$\mathcal{PT}$-symmetry phase transition in the magnon–cavity–magnon coupled system, *Phys. Rev. Applied* 13, 014053 (2020)

22. Y. Yang, Y.-P. Wang, J. W. Rao, Y. S. Gui, B. M. Yao, W. Lu, and C.-M. Hu, Unconventional singularity in anti-parity–time symmetric cavity magnonics, *Phys. Rev. Lett.* 125, 147202 (2020)

23. Y. Cao and P. Yan, Exceptional magnetic sensitivity of $\mathcal{PT}$-symmetric cavity magnon polaritons, *Phys. Rev. B* 99, 214415 (2019)

24. X. Zhang, K. Ding, X. Zhou, J. Xu, and D. Jin, Experimental observation of an exceptional surface in synthetic dimensions with magnon polaritons, *Phys. Rev. Lett.* 123, 237202 (2019)

25. J. M. P. Nair, D. Mukhopadhyay, and G. S. Agarwal, Enhanced sensing of weak anharmonicities through coherences in dissipatively coupled anti-$\mathcal{PT}$ symmetric systems, *Phys. Rev. Lett.* 126, 180401 (2021)

26. B. Wang, Z.-X. Liu, C. Kong, H. Xiong, and Y. Wu, Magnon-induced transparency and amplification in $\mathcal{PT}$-symmetric cavity-magnon system, *Opt. Express* 26, 20248 (2018)

27. B. Wang, C. Kong, Z.-X. Liu, H. Xiong, and Y. Wu, Magnetic-field-controlled magnon chaos in an active cavity-magnon system, *Laser Phys. Lett.* 16, 045208 (2019)

28. Z.-X. Liu, C. You, B. Wang, H. Xiong, and Y. Wu, Phase-mediated magnon chaos-order transition in cavity optomagnonics, *Opt. Lett.* 44, 507 (2019)

29. M. Harder, Y. Yang, B. M. Yao, C. H. Yu, J. W. Rao, Y. S. Gui, R. L. Stamps, and C.-M. Hu, Level attraction due to dissipative magnon-photon coupling, *Phys. Rev. Lett.* 121, 137203 (2018)

30. B. Bhoi, B. Kim, S.-H. Jang, J. Kim, J. Yang, Y.-J. Cho, and S.-K. Kim, Abnormal anticrossing effect in photon–magnon coupling, *Phys. Rev. B* 99, 134426 (2019)

31. Y. Yang, J. W. Rao, Y. S. Gui, B. M. Yao, W. Lu, and C.-M. Hu, Control of the Magnon–photon level attraction in a planar cavity, *Phys. Rev. Applied* 11, 054023 (2019)

32. J. W. Rao, C. H. Yu, Y. T. Zhao, Y. S. Gui, X. L. Fan, D. S. Xue, and C.-M. Hu, Level attraction and level repulsion of magnon coupled with a cavity anti-resonance, *New J. Phys.* 21, 065001 (2019)

33. Y.-P. Wang, J. W. Rao, Y. Yang, P.-C. Xu, Y. S. Gui, B. M. Yao, J. Q. You, and C.-M. Hu, Nonreciprocity and unidirectional invisibility in cavity magnonics, *Phys. Rev. Lett.* 123, 127202 (2019)

34. W. Yu, J. Wang, H. Y. Yuan, and J. Xiao, Prediction of attractive level crossing via a dissipative mode, *Phys. Rev. Lett.* 123, 227201 (2019)

35. Bimu Yao, Tao Yu, Y. S. Gui, J. W. Rao, Y. T. Zhao, W. Lu, and C.-M. Hu, Coherent control of magnon radiative damping with local photon states, *Commun. Phys.* 2, 161 (2019)

36. B. Yao, T. Yu, X. Zhang, W. Lu, Y. Gui, C.-M. Hu, and Y. M. Blanter, The microscopic origin of magnon–photon level attraction by traveling waves: Theory and experiment, *Phys. Rev. B* 100, 214426 (2019)

37. J. W. Rao, Y. P. Wang, Y. Yang, T. Yu, Y. S. Gui, X. L. Fan, D. S. Xue, and C.-M. Hu, Interactions between a magnon mode and a cavity photon mode mediated by traveling photons, *Phys. Rev. B* 101, 064404 (2020)

38. Y.-P. Wang and C.-M. Hu, Dissipative couplings in cavity magnonics, *J. Appl. Phys.* 127, 130901 (2020)

39. I. Proskurin, R. Macêdo, and R. L. Stamps, Microscopic origin of level attraction for a coupled magnon–photon system in a microwave cavity, *New J. Phys.* 21, 095003 (2019)

40. A. Osada, A. Gloppe, Y. Nakamura, and K. Usami, Orbital angular momentum conservation in Brillouin light scattering within a ferromagnetic sphere, *New J. Phys.* 20, 103018 (2018)

42201-16

Kai Wang, et al., Front. Phys. 17(4), 42201 (2022)

41. A. Osada, A. Gloppe, R. Hisatomi, A. Noguchi, R. Ya-mazaki, M. Nomura, Y. Nakamura, and K. Usami, Bril-louin light scattering by magnetic quasivortices in cavity optomagnonics, *Phys. Rev. Lett.* 120, 133602 (2018)

42. J. A. Haigh, N. J. Lambert, S. Sharma, Y. M. Blanter, G. E. W. Bauer, and A. J. Ramsay, Selection rules for cavity-enhanced Brillouin light scattering from magnetostatic modes, *Phys. Rev. B* 97, 214423 (2018)

43. A. Gloppe, R. Hisatomi, Y. Nakata, Y. Nakamura, and K. Usami, Resonant magnetic induction tomography of a magnetized sphere, *Phys. Rev. Applied* 12, 014061 (2019)

44. J. Graf, H. Pfeifer, F. Marquardt, and S. V. Kusminskiy, Cavity optomagnonics with magnetic textures: Coupling a magnetic vortex to light, *Phys. Rev. B* 98, 241406 (2018)

45. S. Sharma, B. Z. Rameshti, Y. M. Blanter, and G. E. W. Bauer, Optimal mode matching in cavity optomagnonics, *Phys. Rev. B* 99, 214423 (2019)

46. P. A. Pantazopoulos, N. Stefanou, E. Almpanis, and N. Papanikolaou, Photomagnonic nanocavities for strong light–spin-wave interaction, *Phys. Rev. B* 96, 104425 (2017)

47. P. A. Pantazopoulos, K. L. Tsakmakidis, E. Almpanis, G. P. Zouros, and N. Stefanou, High-efficiency triple-resonant inelastic light scattering in planar optomagnonic cavities, *New J. Phys.* 21, 095001 (2019)

48. P. A. Pantazopoulos and N. Stefanou, Planar opto-magnonic cavities driven by surface spin waves, *Phys. Rev. B* 101, 134426 (2020)

49. J. A. Haigh, R. A. Chakalov, and A. J. Ramsay, Subpico-liter magnetoptical cavities, *Phys. Rev. Appl.* 14, 044005 (2020)

50. S. V. Kusminskiy, H. X. Tang, and F. Marquardt, Cou-pled spin-light dynamics in cavity optomagnonics, *Phys. Rev. A* 94, 033821 (2016)

51. Y.-P. Gao, C. Cao, Y.-W. Duan, X.-F. Liu, T.-T. Pang, T.-J. Wang, and C. Wang, Magnons scattering in-duced photonic chaos in the optomagnonic resonators, *Nanophotonics* 9(7), 1953 (2020)

52. Y.-P. Gao, X.-F. Liu, T.-J. Wang, C. Cao, and C. Wang, Photon excitation and photon-blockade effects in opto-magnonic microcavities, *Phys. Rev. A* 100, 043831 (2019)

53. W.-L. Xu, X.-F. Liu, Y. Sun, Y.-P. Gao, T.-J. Wang, and C. Wang, Magnon-induced chaos in an optical $\mathcal{PT}$-symmetric resonator, *Phys. Rev. E* 101, 012205 (2020)

54. W.-L. Xu, Y.-P. Gao, C. Cao, T.-J. Wang, and C. Wang, Nanoscatterer-mediated frequency combs in cavity opto-magnonics, *Phys. Rev. A* 102, 043519 (2020)

55. W.-L. Xu, Y.-P. Gao, T.-J. Wang, and C. Wang, Magnon-induced optical high-order sideband generation in hy-brid atom-cavity optomagnonical system, *Opt. Express* 28, 22334 (2020)

56. A. Mahmoud, F. Ciubotaru, F. Vanderveken, A. V. Chu-mak, S. Hamdioui, C. Adelmann, and S. Cotofana, In-troduction to spin wave computing, *J. Appl. Phys.* 128, 161101 (2020)

57. L. Landau and E. Lifshitz, On the theory of the dispersion of magnetic permeability in ferromagnetic bodies, *Phys. Z. Sowjetunion* 8, 101 (1935)

58. T. L. Gilbert, A phenomenological theory of damping in ferromagnetic materials, *IEEE Trans. Magn.* 40, 3443 (2004)

59. I. S. Maksymov and M. Kostylev, Broadband stripline ferromagnetic resonance spectroscopy of ferromagnetic films, multilayers and nanostructures, *Physica E* 69, 253 (2015)

60. T. Holstein and H. Primakoff, Field dependence of the intrinsic domain magnetization of a ferromagnet, *Phys. Rev.* 58, 1098 (1940)

61. M. Goryachev, W. G. Farr, D. L. Creedon, Y. Fan, M. Kostylev, and M. E. Tobar, High-cooperativity cavity QED with magnons at microwave frequencies, *Phys. Rev. Appl.* 14, 044005 (2014)

62. D. Zhang, X.-M. Wang, T.-F. Li, X.-Q. Luo, W. Wu, F. Nori, and J. Q. You, Cavity quantum electrodynam-ics with ferromagnetic magnons in a small yttrium-iron-garnet sphere, *npj Quantum Inf.* 1, 15014 (2015)

63. N. Kostylev, M. Goryachev, and M. E. Tobar, Super-strong coupling of a microwave cavity to yttrium iron garnet magnons, *Appl. Phys. Lett.* 108, 062402 (2016)

64. J. Bourhill, N. Kostylev, M. Goryachev, D. L. Creedon, and M. E. Tobar, Ultrahigh cooperativity interactions be-tween magnons and resonant photons in a YIG sphere, *Phys. Rev. B* 93, 144420 (2016)

65. A. Guo, G. J. Salamo, D. Duchesne, R. Morandotti, M. Volatier-Ravat, V. Aimez, G. A. Siviloglou, and D. N. Christodoulides, Observation of $\mathcal{PT}$-symmetry break-ing in complex optical potentials, *Phys. Rev. Lett.* 103, 093902 (2009)

66. C. E. Rüter, K. G. Makris, R. El-Ganainy, D. N. Christodoulides, M. Segev, and D. Kip, Observation of parity–time symmetry in optics, *Nat. Phys.* 6, 192 (2010)

67. A. Regensburger, C. Bersch, M.-A. Miri, G. Onishchukov, D. N. Christodoulides, and U. Peschel, Parity–time syn-thetic photonic lattices, *Nat. Phys.* 488, 167 (2012)

68. B. Peng, Ş. K. Özdemir, F. Lei, F. Monifi, M. Gianfreda, G. L. Long, S. Fan, F. Nori, C. M. Bender, and L. Yang, Parity–time-symmetric whispering-gallery microcavities, *Nat. Phys.* 10, 394 (2014)

69. P. Peng, W. Cao, C. Shen, W. Qu, J. Wen, L. Jiang, and Y. Xiao, Anti-parity–time symmetry with flying atoms, *Nat. Phys.* 12, 1139 (2016)

70. Y. Choi, C. Hahn, J. W. Yoon, and S. H. Song, Ob-servation of an anti-$\mathcal{PT}$-symmetric exceptional point and energy-difference conserving dynamics in electrical circuit resonators, *Nat. Commun.* 9, 2182 (2018)

71. H. Y. Yuan, P. Yan, S. Zheng, Q. Y. He, Ke Xia, and M.-H. Yung, Steady bell state generation via magnon–photon coupling, *Phys. Rev. Lett.* 124, 053602 (2020)

72. C. Liu, Z. Dutton, C. H. Behroozi, and L. V. Hau, Ob-servation of coherent optical information storage in an atomic medium using halted light pulses, *Nature* 409, 490 (2001)

73. R. W. Boyd, D. J. Gauthier, and A. L. Gaeta, Applica-tions of slow light in telecommunications, *Optics Photon. News.* 17(4), 18 (2006)

74. S. Rajput, V. Kaushik, S. Jain, and M. Kumar, Slow light enhanced phase shifter based on low-loss silicon-ITO hollow waveguide, *IEEE Photon. J.* 11, 1 (2019)

Kai Wang, et al., Front. Phys. 17(4), 42201 (2022)

42201-17

75. Y. Hinakura, Y. Terada, H. Arai, and T. Baba, Electro-optic phase matching in a Si photonic crystal slow light modulator using meander-line electrodes, *Opt. Express* 26, 11538 (2018)

76. K. Qian, F. Wang, R. Wang, S. Zhen, X. Wu, G. Tu, T. Zhang, B. Yu, and L. Zhan, Enhanced sensitivity of fiber laser sensor with Brillouin slow light, *Opt. Express* 27, 25485 (2019)

77. M. F. Yanik, W. Suh, Z. Wang, and S. Fan, Stopping light in a waveguide with an all-optical analog of electromagnetically induced transparency, *Phys. Rev. Lett.* 93, 233903 (2004)

78. D. Tarhan, S. Huang, and Ö. E. Müstecaplıoğlu, Superluminal and ultraslow light propagation in optomechanical systems, *Phys. Rev. A* 87, 013824 (2013)

79. B. Wang, Z.-X. Liu, C. Kong, H. Xiong, and Y. Wu, Mechanical exceptional-point-induced transparency and slow light, *Opt. Express* 27, 8069 (2019)

80. Q. He, F. Badshah, R. U. Din, H. Zhang, Y. Hu, and G.-Q. Ge, Optomechanically induced transparency and the long-lived slow light in a nonlinear system, *J. Opt. Soc. Am. B* 35, 1649 (2018)

81. Z. Liu, H. Xiong, and Y. Wu, Room-temperature slow light in a coupled cavity magnon-photon system, *IEEE Access* 7, 57047 (2019)

82. C.-Z. Liu, Y.-L. Deng, and M. Yin, Relative-cavity-length-controlled slow light in a cascaded magnon–photon system, *J. Opt. Soc. Am. B* 37, 1127 (2020)

83. J. Z., L. Wu, T. Li, Y.-X. Liu, F. Nori, Y. Liu, and J. Du, Phase-controlled pathway interferences and switchable fast-slow light in a cavity-magnon polariton system, *Phys. Rev. Applied* 15, 024056 (2021)

84. L. Bai, P. Hyde, Y. S. Gui, C.-M. Hu, V. Vlaminck, J. E. Pearson, S. D. Bader, and A. Hoffmann, Universal method for separating spin pumping from spin rectification voltage of ferromagnetic resonance, *Phys. Rev. Lett.* 111, 217602 (2013)

85. L. Bai, M. Harder, Y. P. Chen, X. Fan, J. Q. Xiao, and C.-M. Hu, Spin pumping in electrodynamically coupled magnon–photon systems, *Phys. Rev. Lett.* 114, 227201 (2015)

86. L. Ba, M. Harder, P. Hyde, Z. Zhang, C.-M. Hu, Y. P. Chen, and J. Q. Xiao, Cavity mediated manipulation of distant spin currents using a cavity-magnon-polariton, *Phys. Rev. Lett.* 118, 217201 (2017)

87. T. A. Palomaki, J. D. Teufel, R. W. Simmonds, and K. W. Lehnert, Entangling mechanical motion with microwave fields, *Science* 342, 710 (2013)

88. S. G. Hofer, W. Wieczorek, M. Aspelmeyer, and K. Hammerer, Quantum entanglement and teleportation in pulsed cavity optomechanics, *Phys. Rev. A* 84, 052327 (2011)

89. U. Akram, W. Munro, K. Nemoto, and G. J. Milburn, Photon–phonon entanglement in coupled optomechanical arrays, *Phys. Rev. A* 86, 042306 (2012)

90. M. Ho, E. Oudot, J.-D. Bancal, and N. Sangouard, Witnessing optomechanical entanglement with photon counting, *Phys. Rev. Lett.* 121, 023602 (2018)

91. H. Tan, G. Li, and P. Meystre, Dissipation-driven two-mode mechanical squeezed states in optomechanical systems, *Phys. Rev. A* 87, 033829 (2013)

92. G. Huang, W. Deng, H. Tan, and G. Cheng, Generation of squeezed states and single-phonon states via homodyne detection and photon subtraction on the filtered output of an optomechanical cavity, *Phys. Rev. A* 99, 043819 (2019)

93. J. Li, S.-Y. Zhu, and G. S. Agarwal, Magnon–photon–phonon entanglement in cavity magnomechanics, *Phys. Rev. Lett.* 121, 203601 (2018)

94. Z.-B. Yang, J.-S. Liu, H. Jin, Q.-H. Zhu, A.-D. Zhu, H.-Y. Liu, Y. Ming, and R.-C. Yang, Entanglement enhanced by Kerr nonlinearity in a cavity-optomagnonics system, *Opt. Express* 28, 31862-31871 (2020)

95. J. Li, S.-Y. Zhu, and G. S. Agarwal, Squeezed states of magnons and phonons in cavity magnomechanics, *Phys. Rev. A* 99, 021801 (2019)

96. W. Zhang, D.-Y. Wang, C.-H. Bai, T. Wang, S. Zhang, and H.-F. Wang, Generation and transfer of squeezed states in a cavity magnomechanical system by two-tone microwave fields, *Opt. Express* 29, 11773 (2021)

97. J. R. Eshbach and R. W. Damon, Surface magnetostatic modes and surface spin waves, *Phys. Rev.* 118, 1208 (1960)

98. R. W. Damon and J. R. Eshbach, Magnetostatic modes of a ferromagnet slab, *J. Phys. Chem. Solids* 19, 308 (1961)

99. J. Graf, S. Sharma, H. Huebl, and S. V. Kusminskiy, Design of an optomagnonic crystal: Towards optimal magnon–photon mode matching at the microscale, *Phys. Rev. Research* 3, 013277 (2021)

100. T. Liu, X. Zhang, H. X. Tang, and M. E. Flatté, Optomagnonics in magnetic solids, *Phys. Rev. B* 94, 060405 (2016)

101. Y.-P. Gao, C. Cao, T.-J. Wang, Y. Zhang, and C. Wang, Cavity-mediated coupling of phonons and magnons, *Phys. Rev. A* 96, 023826 (2017)

102. V. A. S. V. Bittencourt, V. Feulner, and S. Viola Kusminskiy, Magnon heralding in cavity optomagnonics, *Phys. Rev. A* 100, 013810 (2019)

103. H. Dery, P. Dalal, Ł. Cywiński, and L. J. Sham, Spin-based logic in semiconductors for reconfigurable large-scale circuits, *Nature* 447, 573 (2007)

104. V. E. Demidov, S. Urazhdin, R. Liu, B. Divinskiy, A. Telegin, and S. O. Demokritov, Excitation of coherent propagating spin waves by pure spin currents, *Nat. Commun.* 7, 10446 (2016)

105. Y. Kajiwara, K. Harii, S. Takahashi, J. Ohe, K. Uchida, M. Mizuguchi, H. Umezawa, H. Kawai, K. Ando, K. Takanashi, S. Maekawa, and E. Saitoh, Transmission of electrical signals by spin-wave interconversion in a magnetic insulator, *Nature* 464, 262 (2010)

106. V. E. Demidov, H. Ulrichs, S. V. Gurevich, S. O. Demokritov, V. S. Tiberkevich, A. N. Slavin, A. Zholud, and S. Urazhdin, Synchronization of spin Hall nano-oscillators to external microwave signals, *Nat. Commun.* 5, 3179 (2014)

42201-18

Kai Wang, et al., Front. Phys. 17(4), 42201 (2022)

107. G. Talmelli, F. Ciubotaru, K. Garello, X. Sun, M. Heyns, I. P. Radu, C. Adelmann, and T. Devolder, Spin-wave emission by spin–orbit-torque antennas, *Phys. Rev. Appl.* 10, 044060 (2018)

108. X. Zhang, A. Galda, X. Han, D. Jin, and V. M. Vinokur, Broadband nonreciprocity enabled by strong coupling of magnons and microwave photons, *Phys. Rev. Appl.* 13, 044039 (2020)

109. A. Kord, D. L. Sounas, and A. Alù, Microwave nonreciprocity, *Proc. IEEE* 108, 1728 (2020)

110. N. Crescini, C. Braggio, G. Carugno, R. Di Vora, A. Ortolan, and G. Ruoso, Magnon-driven dynamics of a hybrid system excited with ultrafast optical pulses, *Commun. Phys.* 3, 164 (2020)

111. Q. Cai, J. Liao, and Q. Zhou, Stationary entanglement between light and microwave via ferromagnetic magnons, *Ann. Phys.* 532, 2000250 (2020)

112. D.-W. Luo, X.-F. Qian, and T. Yu, Nonlocal magnon entanglement generation in coupled hybrid cavity systems, *Opt. Lett.* 46, 1073 (2021)

113. S. Sharma, V. A. S. V. Bittencourt, A. D. Karenowska, and S. V. Kusminskiy, Spin cat states in ferromagnetic insulators, *Phys. Rev. B* 103, L100403 (2021)

114. Y. Tabuchi, S. Ishino, A. Noguchi, T. Ishikawa, R. Yamazaki, K. Usami, and Y. Nakamura, Coherent coupling between a ferromagnetic magnon and a superconducting qubit, *Science* 349, 405 (2015)

Kai Wang, et al., Front. Phys. 17(4), 42201 (2022)

42201-19